

Stellar core collapse in full general relativity with microphysics – Formulation and Spherical collapse test –

Yuichiro SEKIGUCHI

*Division of Theoretical Astronomy, National Astronomical Observatory of Japan,
Mitaka, Tokyo 181-8588, Japan*

One of the longstanding issues in numerical relativity is to enable a simulation taking account of microphysical processes (e.g., weak interactions and neutrino cooling). We develop an approximate and explicit scheme in the fully general relativistic framework as a first implementation of the microphysics toward a more realistic and sophisticated modeling. In this paper, we describe in detail a method for implementation of a realistic equation of state, the electron capture and the neutrino cooling in a multidimensional, fully general relativistic code. The procedure is based on the so-called neutrino leakage scheme. To check the validity of the code, we perform a two dimensional (2D) simulation of spherical stellar core collapse. Until the convective activities set in, our results approximately agree, or at least are consistent, with those in the previous so-called state-of-the-art simulations. In particular, the radial profiles of thermodynamical quantities and the time evolution of the neutrino luminosities agree quantitatively. The convection is driven by negative gradients of the entropy per baryon and the electron fraction as in the previous 2D Newtonian simulations. We clarify which gradient is more responsible for the convection. Gravitational waves from the convection are also calculated. We find that the characteristic frequencies of the gravitational-wave spectra are distributed for higher frequencies than those in Newtonian simulations due to the general relativistic effects.

§1. Introduction

1.1. Motivation

Gravitational collapse of massive stellar core to a neutron star or a black hole and the associated supernova explosion are one of the important and interesting events in the universe. From observational view point, they are among the most energetic events in astrophysics, producing a wide variety of observable signatures, namely, electromagnetic radiation, neutrinos, and gravitational radiation.

Most of the energy liberated in the collapse is eventually carried away by neutrinos from the system. The total energy of neutrinos emitted is $\approx GM_{\text{NS}}^2/R_{\text{NS}} \sim 0.1M_{\text{NS}}c^2 \sim$ several times 10^{53} ergs, where M_{NS} and R_{NS} are the mass and radius of the neutron star. Observations of gravitational collapse by neutrino detectors will provide important information of the deep inside of the core, because neutrinos can propagate from the central regions of the stellar core almost freely due to their small cross-sections with matters. Electromagnetic radiation, by contrast, interacts strongly with matters and thus gives information of collapse coming only from lower-density regions near the surface of the star. Bursts of neutrinos were first detected simultaneously by the Kamiokande¹⁾ and Irvine-Michigan-Brookhaven²⁾ facilities in the supernova SN1987A, which occurred on February 23, 1987 in the Large Magellanic Cloud (for a review, see Ref. 3)). Future detection of neutrinos will provide a

direct clue to reveal the physical ingredient for the supernova explosion mechanism.

Gravitational wave astronomy will start in this decade. The first generation of ground-based interferometric detectors (LIGO,⁴⁾ VIRGO,⁵⁾ GEO600,⁶⁾ TAMA300⁷⁾) are now in the scientific search for gravitational waves. Stellar core collapse is one of the important sources for these observatories. Observations of gravitational collapse by gravitational-wave detectors will provide unique information, complementary to that derived from electromagnetic and neutrino detectors, because gravitational waves can propagate from the innermost regions of a progenitor star to the detectors without attenuation by matters. Combination of the signatures of neutrinos and gravitational waves will provide much information about processes of the core collapse and ultimately, the physics that governs the stellar core collapse.

To obtain physically valuable information from these observations, it is necessary to connect the observed data and the physics behind it. For this purpose, a numerical simulation is the unique approach. However, simulating the stellar core collapse is one of the challenging problems because a rich diversity of physics has to be taken into account. All four known forces in nature are involved and play important roles during the collapse. General relativistic gravity plays an essential role in formation of a black hole and a neutron star. The weak interactions govern energy and lepton-number losses of the system. In particular, neutrinos transport most of the energy released during the collapse to the outside of the system. The electromagnetic and strong interactions determine the ingredient of the collapsing matter and the thermodynamical properties of the dense matter. Strong magnetic fields, if they are present, would modify the dynamics of the collapse, subsequent supernova explosion, and evolution of proto-neutron stars.

Due to these complexities, the explosion mechanism of core-collapse supernovae has not been fully understood in spite of the elaborate effort in the past about 40 years.^{8),9),10)} Recent numerical studies^{11),12),13),14),15),16)} have clarified that on the assumption of the spherical symmetry, the explosion does not succeed for the iron core collapse with the currently most elaborate input physics (neutrino interactions, neutrino transfer, and equation of states of the dense matter) on the basis of the standard “neutrino heating mechanism”¹⁰⁾ (but see Ref. 17) for successful explosion in O-Ne-Mg core collapse). To increase the neutrino-heating efficiency, a wide variety of multi-dimensional effects have been explored (for recent reviews, see e.g., Refs. 9), 8) and also Refs. 18) and 19) for simulations where successful explosions are obtained). However, it has not been completely clarified yet whether the increase of the heating efficiency due to such multi-dimensional effects suffices for yielding successful explosion, because the explosion energy resulting from these works is too low $\sim 10^{50}$ ergs.

Similarly, accurate predictions of gravitational waveforms are still hampered by the facts that reliable estimates of waveforms require a general relativistic treatment,²⁰⁾ and that appropriate treatments of microphysics such as nuclear equation of state (EOS), the electron capture, and neutrino emissions and transfers. Indeed, previous estimates of waveforms have relied either on Newtonian simulations with including microphysics to some extent,^{21),22),23),24),25),26),27),28)} or general relativistic simulations with simplified microphysics.^{20),29),30),31),32)} Recently, gravitational

waveforms emitted in the rotating core collapse were derived by multidimensional simulations in general relativistic frameworks^{33),34)} adopting a finite-temperature nuclear EOS³⁵⁾ and the electron capture. In their studies, however, the electron capture rate was not calculated in a self-consistent manner. Instead, they adopted a simplified prescription proposed in Ref. 36) which is based on the result of a spherically symmetric simulation. However, it is not clear whether this treatment is justified for non-spherical collapse or not. Moreover, they did not take account of emission processes of neutrinos. More sophisticated simulations including microphysics are required to make accurate predictions of gravitational waveforms.

The gravitational collapse of massive star is also the primary mechanism of black hole formation. Understanding the process of black hole formation is one of the most important issues in the theory of the stellar core collapse. A wide variety of recent observations have shown that black holes actually exist in the universe (e.g., see Ref. 37)), and so far, about 20 stellar-mass black holes for which the mass is determined within a fairly small error have been observed in binary systems of our Galaxy and the Large Magellanic Clouds.³⁸⁾ The formation of a black hole through the gravitational collapse is a highly nonlinear and dynamical phenomenon, and therefore, numerical simulation in full general relativity is the unique approach to this problem. In spherical symmetry, fully general relativistic simulations of stellar core collapse to a black hole have been performed in a state-of-the-art manner, i.e., employing realistic EOSs, implementing microphysical processes, and the Boltzmann transfer of neutrinos.^{39),40)} In the multidimensional case, by contrast, simulations only with simplified microphysics have been performed.^{30),41),42)} Because multidimensional effects such as rotation and convection are likely to play an important role, multidimensional simulations in full general relativity employing a realistic EOS and detailed microphysics are necessary for clarifying the formation process of black holes.

Furthermore, recent observations^{43),44),45)} have found the spectroscopic connections between several SNe and long gamma-ray bursts (GRBs) and clarified that some of long GRBs are associated with the collapse of massive stars. Supported by these observations, the collapsar model⁴⁶⁾ is currently one of promising models for the central engine of GRBs. In this model, one assumes that the central engine of the long GRBs is composed of a rotating black hole and a hot, massive accretion disk. Such a system may be formed as a result of the collapse of rapidly rotating massive core. In this model, one of the promising processes of the energy-deposition to form a GRB fireball is the pair annihilation of neutrinos emitted from the hot, massive disk ($\nu_e + \bar{\nu}_e \rightarrow e^- + e^+$). The collapsar model requires the progenitor core to be rotating rapidly enough that the massive accretion disk can be formed around the black hole. Recent general relativistic numerical analyses have shown that if a progenitor of the collapse is massive and the angular momentum is large enough, a black hole surrounded by a massive disk will be formed.^{47),48),41)} However, the formation mechanism of such system has not been clarified in detail. These also enhance the importance of exploring the stellar core collapse to a black hole taking account of microphysical processes.

As reviewed above, multidimensional simulations of stellar collapse in full gen-

eral relativity including microphysics is currently one of the most required subjects in theoretical astrophysics. However, there has been no multidimensional code in full general relativity that self-consistently includes microphysics such as realistic EOS, electron capture, and neutrino emission. There have only existed fully general relativistic codes in spherical symmetry^{49), 50), 16)} or Newtonian codes in multidimension.^{11), 12), 13)} We have developed a fully general relativistic multidimensional code including a finite-temperature nuclear EOS, self-consistent treatment of the electron capture, and a simplified treatment of neutrino emission for the first time. In this code, by contrast with the previous ones,^{33), 34)} the electron capture rate is treated in a self-consistent manner and the neutrino cooling is taken into account for the first time. Because it is not currently feasible to fully solve the neutrino transfer equations in the framework of general relativity in multidimension because of restrictions of computational resources, it will be reasonable to take some approximation for the transfer equations at the current status. In this paper, the so-called neutrino leakage scheme is adopted as an approximate treatment of neutrino cooling, and a general relativistic version of the leakage scheme is developed.

1.2. The leakage schemes

The neutrino leakage schemes^{51), 52), 53), 54), 55), 56), 57), 58)} as an approximate method for the neutrino cooling have a well-established history (e.g. Ref. 57)). The basic concept of the original neutrino leakage schemes^{51), 52)} is to treat the following two regions in the system separately: one is the region where the diffusion timescale of neutrinos is longer than the dynamical timescale, and hence, neutrinos are 'trapped' (neutrino-trapped region); the other is the region where the diffusion timescale is shorter than the dynamical timescale, and hence, neutrinos stream out freely out of the system (free-streaming region). The idea of treating the diffusion region separately has been applied to more advanced methods for the neutrino transfer (see e.g., Ref. 59) and references therein).

Then, electron neutrinos and electron anti-neutrinos in the neutrino-trapped region are assumed to be in the β -equilibrium state. The *net* local rates of lepton-number and energy exchange with matters are set to be zero in the neutrino-trapped region. To treat diffusive emission of neutrinos leaking out of the neutrino-trapped region, simple phenomenological source terms based on the diffusion theory are introduced.^{51), 52)} In the free-streaming region, on the other hand, it is assumed that neutrinos escape from the system without interacting with matters. Therefore, neutrinos carry the lepton number and the energy according to the local weak-interaction rates. Note that the neutrino fractions are not solved in the original version of the leakage scheme: Only the total lepton fraction (from which the neutrino fractions are calculated under the β -equilibrium condition) is necessary in the neutrino-trapped region, and the neutrino fractions are set to be zero in the free-streaming region. As a result, neutrino quantities and the electron fraction are discontinuous at the boundary the neutrino-trapped and free-streaming regions.

The boundary was given by hand as a single 'neutrino-trapping' density (ρ_{trap}) without calculating the optical depths of neutrinos in the previous studies.^{51), 52), 53), 54), 55), 58)} However, the location at which the neutrino trapping occurs in fact depends strongly

on the neutrino energies (E_ν) as⁶⁰⁾ $\rho_{\text{trap}} \propto E_\nu^{-3}$, and hence, there are different neutrino-trapping densities for different neutrino energies. In the previous leakage schemes,^{51), 52), 53), 54), 58)} on the other hand, all neutrinos were emitted in one moment irrespective of their energy. Consequently in the case of the so-called neutrino burst emission (e.g., Ref. 60)), for example, the duration in which the neutrinos are emitted was shortened and the peak luminosity at the burst was overestimated.^{53), 58), 61)} The dependence of the neutrino-trapping densities and the neutrino diffusion rates on the neutrino energies are approximately taken into account in the recent simulations of mergers of binary neutron star.^{63), 62)} However, the lepton-number conservation equations for neutrinos are not solved,⁶³⁾ which is important to estimate the phase space blocking due to neutrinos.

Transfer equations of neutrinos are not solved in the leakage schemes. Therefore, the leakage schemes cannot treat *non-local* interactions among the neutrinos and matters. For example, the so-called neutrino heating⁶⁴⁾ and the neutrino pair annihilation cannot be treated in the leakage scheme. Nevertheless, we believe a detailed general relativistic leakage scheme presented in this paper to be a valuable approach because even by this approximated approach it is possible to incorporate the effects of neutrinos semi-quantitatively as shown in this paper. Also, the neutrino leakage scheme is an appropriate method for studying a number of phenomena for which the neutrino heating and neutrino transfer are expected to be not very important, e.g., prompt formation of a black hole and compact binary mergers. Both of these phenomena are the targets of the present code.

A first attempt towards a general relativistic leakage scheme was done in the previous study.⁶¹⁾ In that study, not the region of the system but the energy momentum tensor of neutrinos was decomposed into two parts; 'trapped-neutrino' and 'streaming-neutrino' parts. However the source terms of hydrodynamic and lepton-number-conservation equations were determined using the single neutrino-trapping density as in the case of the previous leakage schemes. In this paper, we develop a new code implementing the microphysical processes in the general relativistic framework based on the previous study.⁶¹⁾ As an application of the code, we perform simulations of stellar core collapse.

A lot of improved ingredients are installed into the present code: (1) The dependence of the neutrino diffusion rates on the neutrino energies are approximately taken into account following the recent study⁶²⁾ with detailed cross sections, instead of adopting the single neutrino-trapping density (see Appendix C). (2) The lepton-number conservation equations for neutrinos are solved to calculate self-consistently the chemical potentials of neutrinos. Then, the blocking effects due to the presence of neutrinos and the β -equilibrium condition can be taken into account more accurately (see §3). (3) A stable explicit method for solving the equations of hydrodynamics, the lepton-number conservations, and neutrinos are developed. Such a special procedure is necessary because the characteristic timescale of the weak-interaction processes (hereafter referred to as the WP timescale $t_{\text{wp}} \sim |Y_e/\dot{Y}_e|$) is much shorter than the dynamical timescale t_{dyn} in hot, dense matter regions.^{65), 62)} Note that in the previous leakage schemes,^{51), 52), 53), 54), 58)} the β -equilibrium was assumed to be achieved in such regions (i.e. $\dot{Y}_e = 0$) and no such special treatments

are required. See §2 for further discussions and §3 for details of the method. (4) The electron capture rate are calculated in a detailed manner⁶⁶⁾ including effects of the so-called thermal unblocking⁶⁷⁾ (see Appendix A).

The paper is organized as follows. First, issues in implementation of weak interactions and neutrino cooling in full general relativistic simulation is briefly summarized in §2. Then, framework of the general relativistic leakage scheme is described in detail in § 3. In § 4, EOSs employed in this paper are described in some details. Basic equations and numerical methods of the simulations are described in § 5. Numerical results obtained in this paper are shown in § 6. We devote § 7 to a summary and discussions. In appendices, details of the microphysics adopted in the present paper are summarized for the purpose of convenience. Throughout the paper, the geometrical unit $c = G = 1$ is used otherwise stated.

§2. Issues in implementation of weak interactions and neutrino cooling in fully general relativistic simulation

Because the characteristic timescale of the weak-interaction processes (the WP timescale $t_{\text{wp}} \sim |Y_e/\dot{Y}_e|$) is much shorter than the dynamical timescale t_{dyn} in hot dense matters,^{65),62)} the *explicit* numerical treatments of the weak interactions are computationally expensive in simple methods, as noted in the previous pioneering work by Bruenn:⁶⁵⁾ A very short timestep ($\Delta t < t_{\text{wp}} \ll t_{\text{dyn}}$) will be required to solve the equations explicitly.

The *net* rates of lepton-number and energy exchanges between matters and neutrinos may not be large, and consequently, an *effective* timescale may not be as short as the dynamical timescale. However, this does not immediately imply that one can solve the equations explicitly without employing any prescription. For example, the achievement of β -equilibrium, where $\dot{Y}_e = 0$ is the consequence of the cancellation of two very *large* weak interaction processes (the electron and the electron-neutrino captures, see Eq. (3·20)) and of the action of the phase space blocking. Note that the weak interaction processes depend enormously both on the temperature and the lepton chemical potentials. Therefore, small error in the evaluation of the temperature and a small deviation from the β -equilibrium due to small error in calculation of the lepton chemical potentials will result in huge error. Then, stiff source terms appear and explicit numerical evolution often becomes unstable. Indeed, we found that a straightforward, explicit solution of the equations did not work.

In the following of this section, we describe issues of implementation of weak interactions and neutrino cooling into the hydrodynamic equations in the conservative schemes in fully general relativistic simulations. First, we illustrate that in the Newtonian framework, the equations may be solved implicitly in a relatively simple manner^{68),65),69),70),14),71),72),73),18)} (see also Refs. 74) and 59) and references therein). The equations of hydrodynamics, lepton-number conservations, and neutrino processes are schematically written as,

$$\dot{\rho} = 0, \tag{2.1}$$

$$\dot{v}_i = S_{v_i}(\rho, Y_e, T, Q_\nu), \tag{2.2}$$

$$\dot{Y}_e = S_{Y_e}(\rho, Y_e, T, Q_\nu), \quad (2.3)$$

$$\dot{e} = S_e(\rho, Y_e, T, Q_\nu), \quad (2.4)$$

$$\dot{Q}_\nu = S_{Q_\nu}(\rho, Y_e, T, Q_\nu), \quad (2.5)$$

where ρ is the rest-mass density, v_i is the velocity, Y_e is the electron fraction, e is the (internal) energy of matter, T is the temperature, and Q_ν stands for the relevant neutrino quantities. We here omit the transport terms. S 's in the right-hand side stand for the relevant source terms. Comparing the quantities in the left-hand-side and the argument quantities in the source terms, only the relation between e and T is nontrivial. Usually, EOSs employed in the simulation are tabularized, and one dimensional search over the EOS table is required to solve them. Due to the relatively simple relations between the quantities to be evolved and the argument quantities, the above equations may be solved implicitly in a straightforward (although complicated) manner.

In the relativistic framework, the situation becomes much more complicated in conservative schemes, because the Lorentz factor (Γ) is coupled with rest-mass density and the energy density (see Eqs. (5.12) and (5.16) where $w \equiv \alpha u^t$ is used instead of Γ), and because the specific enthalpy ($h = h(\rho, Y_e, T)$) is coupled with the momentum (see Eq. (5.14)).

It should be addressed that the previous fully general relativistic works in the spherical symmetry^{49),50)} are based on the so-called Misner-Sharp coordinates.⁷⁵⁾ There are no such complicated couplings in these *Lagrangian* coordinates. Accordingly, the equations may be solved essentially in the same manner as in the Newtonian framework. Because no such simple Lagrangian coordinates are known in the multidimensional case, the complicated couplings inevitably appear in the relativistic framework.

Omitting the factors associated with the geometric variables (which are usually updated before solving the hydrodynamics equations) and the transport terms, the equations to be solved in the general relativistic framework are schematically written as,

$$\dot{\rho}_*(\rho, \Gamma) = 0, \quad (2.6)$$

$$\dot{\hat{u}}_i(u_i, h) = \dot{\hat{u}}_i(u_i, \rho, Y_e, T) = S_{\hat{u}_i}(\rho, Y_e, T, Q_\nu, \Gamma), \quad (2.7)$$

$$\dot{Y}_e = S_{Y_e}(\rho, Y_e, T, Q_\nu, \Gamma), \quad (2.8)$$

$$\dot{e}(\rho, Y_e, T, \Gamma) = S_e(\rho, Y_e, T, Q_\nu, \Gamma), \quad (2.9)$$

$$\dot{Q}_\nu = S_{Q_\nu}(\rho, Y_e, T, Q_\nu, \Gamma), \quad (2.10)$$

where ρ_* is a weighted density, \hat{u}_α is a weighted four velocity, \hat{e} is a weighted energy density (see § 5.2 for the definition of these variables). The Lorentz factor is calculated by solving the normalization condition $u^\alpha u_\alpha = -1$, which is rather complicated nonlinear equation schematically written as

$$f_{\text{normalization}}(\hat{u}_i, \Gamma) = f_{\text{normalization}}(u_i, \rho, Y_e, T, \Gamma) = 0. \quad (2.11)$$

The accurate calculation of the Lorentz factor and the accurate solution of the normalization condition are very important in the numerical relativistic hydrodynamics.

Now, it is obvious that the argument quantities in the source terms are not simply related with the evolved quantities in the left-hand-side of Eqs. (2.6)–(2.11). Solving the equations implicitly is not as straightforward as in the Newtonian case and no successful formulations have been developed. Moreover it might be not clear whether a convergent solution can be *stably* obtained numerically or not, because they are simultaneous nonlinear equations. Therefore, it may be not a poor choice to adopt an alternative approach in which the equations are solved *explicitly* with some approximations as described in the next section*).

§3. General relativistic neutrino leakage scheme

In this section, we describe a method for approximately solving hydrodynamic equations coupled with neutrino radiation in an explicit manner. As described in the previous section, because of the relation $t_{\text{wp}} \ll t_{\text{dyn}}$ in the hot dense matter regions, the source terms in the equations become too *stiff* for the equations to be solved explicitly in the straightforward manner. The characteristic timescale of leakage of neutrinos from the system t_{leak} , by contrast, is much longer than t_{wp} in the hot dense matter region. Rather, $t_{\text{leak}} \sim L/c \sim t_{\text{dyn}}$ where L is the characteristic length scale of the system. On the other hand, t_{leak} is comparable to t_{wp} in the free-streaming regions but t_{wp} is longer than or comparable with t_{dyn} there. All these facts imply that the WP timescale does not directly determine the evolution of the system but the leakage timescale does. Using this fact, we approximate some of original equations and reformulate them so that the source terms are to be characterized by the leakage timescale t_{leak} .

3.1. Decomposition of neutrino energy-momentum tensor

The basic equations of general relativistic hydrodynamics with neutrinos are

$$\nabla_{\alpha}(T^{\text{Total}})^{\alpha}_{\beta} = \nabla_{\alpha}[(T^{\text{F}})^{\alpha}_{\beta} + (T^{\nu})^{\alpha}_{\beta}] = 0, \quad (3.1)$$

where $(T^{\text{Total}})_{\alpha\beta}$ is the total energy-momentum tensor, and $(T^{\text{F}})_{\alpha\beta}$ and $(T^{\nu})_{\alpha\beta}$ are the energy-momentum tensor of fluids and neutrinos, respectively. Equation (3.1) can be written as

$$\nabla_{\alpha}(T^{\text{F}})^{\alpha}_{\beta} = Q_{\beta}, \quad (3.2)$$

$$\nabla_{\alpha}(T^{\nu})^{\alpha}_{\beta} = -Q_{\beta}, \quad (3.3)$$

where the source term Q_{α} is regarded as the local production rate of neutrinos through the weak processes.

Now, the problem is that the source term Q_{α} becomes too stiff to solve explicitly in hot dense matter regions where $t_{\text{wp}} \ll t_{\text{dyn}}$. To overcome this situation, the following procedures are adopted.

First, it is assumed that the energy-momentum tensor of neutrinos are be decomposed into 'trapped-neutrino' $((T^{\nu,\text{T}})_{\alpha\beta})$ and 'streaming-neutrino' $((T^{\nu,\text{S}})_{\alpha\beta})$ parts

*) It should be stated that the implicit schemes are also approximated ones because a short WP timescale associated with the weak interaction is not fully resolved.

as,⁶¹⁾

$$(T^\nu)_{\alpha\beta} = (T^{\nu,T})_{\alpha\beta} + (T^{\nu,S})_{\alpha\beta}. \quad (3.4)$$

Here, the trapped-neutrinos phenomenologically represent neutrinos which interact sufficiently frequently with matter and are thermalized. On the other hand, the streaming-neutrino part describes a phenomenological flow of neutrinos streaming out of the system⁶¹⁾ (see also Ref. 76) where a more sophisticated method in terms of the distribution function is adopted in the Newtonian framework).

Second, the locally produced neutrinos are assumed to *leak out* to be the streaming-neutrinos with a leakage rate Q_α^{leak} :

$$\nabla_\beta (T^{\nu,S})_\alpha^\beta = Q_\alpha^{\text{leak}}. \quad (3.5)$$

Then, the equation of the trapped-neutrino part is

$$\nabla_\beta (T^{\nu,T})_\alpha^\beta = Q_\alpha - Q_\alpha^{\text{leak}}. \quad (3.6)$$

Third, the trapped-neutrino part is combined with the fluid part as

$$T_{\alpha\beta} \equiv (T^F)_{\alpha\beta} + (T^{\nu,T})_{\alpha\beta}, \quad (3.7)$$

and Eqs. (3.2) and (3.6) are combined to give

$$\nabla_\beta T_\alpha^\beta = -Q_\alpha^{\text{leak}}. \quad (3.8)$$

Thus, the equations to be solved are changed from Eqs. (3.2) and (3.3) to Eqs. (3.8) and (3.5). Note that the new equations only include the source term Q_α^{leak} which is characterized by the leakage timescale t_{leak} . Definition of Q_α^{leak} will be given in § 3.3.

The energy-momentum tensor of the fluid and trapped-neutrino parts ($T_{\alpha\beta}$) is treated as that of the perfect fluid,

$$T_{\alpha\beta} = (\rho + \rho\varepsilon + P)u_\alpha u_\beta + P g_{\alpha\beta}, \quad (3.9)$$

where ρ and u^α are the rest mass density and the 4-velocity. The specific internal energy density (ε) and the pressure (P) are the sum of contributions from the baryons (free protons, free neutrons, α -particles, and heavy nuclei), leptons (electrons, positrons, and *trapped-neutrinos*), and the photons as,

$$P = P_B + P_e + P_\nu + P_{ph}, \quad (3.10)$$

$$\varepsilon = \varepsilon_B + \varepsilon_e + \varepsilon_\nu + \varepsilon_{ph}, \quad (3.11)$$

where subscripts ' B ', ' e ', ' ph ', and ' ν ' denote the components of the baryons, electrons and positrons, photons, and trapped-neutrinos, respectively.

The streaming-neutrino part, on the other hand, is set to be a general form of

$$(T^{\nu,S})_{\alpha\beta} = E n_\alpha n_\beta + F_\alpha n_\beta + F_\beta n_\alpha + P_{\alpha\beta}, \quad (3.12)$$

where $F_\alpha n^\alpha = P_{\alpha\beta} n^\alpha = 0$. In order to close the system, we need an explicit expression of $P_{\alpha\beta}$. In this paper, we adopt a simple form $P_{\alpha\beta} = \chi E \gamma_{\alpha\beta}$ with $\chi = 1/3$. This approximation may work well in high density regions but will violate in low density regions. However, the violation will not affect the dynamics because the total amount of streaming-neutrinos emitted in low density regions will be small. Of course, a more sophisticated treatment will be necessary in a future study.

3.2. The lepton-number conservation equations

The conservation equations of the lepton fractions are written schematically as

$$\frac{dY_e}{dt} = -\gamma_e, \quad (3.13)$$

$$\frac{dY_{\nu e}}{dt} = \gamma_{\nu e}, \quad (3.14)$$

$$\frac{dY_{\bar{\nu} e}}{dt} = \gamma_{\bar{\nu} e}, \quad (3.15)$$

$$\frac{dY_{\nu x}}{dt} = \gamma_{\nu x}, \quad (3.16)$$

where Y_e , $Y_{\nu e}$, $Y_{\bar{\nu} e}$, and $Y_{\nu x}$ denote the electron fraction, the electron neutrino fraction, the electron anti-neutrino fraction, and μ and τ neutrino and anti-neutrino fractions, respectively. We note that in the previous simulations based on the leakage schemes,^{51),52),58),63)} the neutrino fractions were not solved.

The source terms of neutrino fractions can be written, on the basis of the present leakage scheme, as

$$\gamma_{\nu e} = \gamma_{\nu e}^{\text{local}} - \gamma_{\nu e}^{\text{leak}}, \quad (3.17)$$

$$\gamma_{\bar{\nu} e} = \gamma_{\bar{\nu} e}^{\text{local}} - \gamma_{\bar{\nu} e}^{\text{leak}}, \quad (3.18)$$

$$\gamma_{\nu x} = \gamma_{\nu x}^{\text{local}} - \gamma_{\nu x}^{\text{leak}}, \quad (3.19)$$

where γ^{local} 's and γ^{leak} 's are the local production and the leakage rates of each neutrino, respectively (see § 3.3). Note that only the trapped-neutrinos are responsible for the neutrino fractions. Assuming that the trapped neutrinos are thermalized and the distribution function is the equilibrium Fermi-Dirac one, the chemical potentials of neutrinos can be calculated from the neutrino fractions. Then the thermodynamical quantities of neutrinos can be also calculated.

The source term of the electron fraction conservation is

$$\gamma_e = \gamma_{\nu e}^{\text{local}} - \gamma_{\bar{\nu} e}^{\text{local}}. \quad (3.20)$$

Because $\gamma_{\nu}^{\text{local}}$'s are characterized by the WP timescale t_{wp} , some procedures are necessary to solve the lepton conservation equations explicitly. The following simple procedures are proposed to solve the equations stably.

First, in each timestep n , the conservation equation of the *total* lepton fraction ($Y_l = Y_e - Y_{\nu e} + Y_{\bar{\nu} e}$),

$$\frac{dY_l}{dt} = -\gamma_l, \quad (3.21)$$

is solved together with the conservation equation of $Y_{\nu x}$, Eq. (3.16), in advance of solving whole of the lepton conservation equations (Eqs. (3.13) – (3.16)). Note that the source term $\gamma_l = \gamma_{\nu e}^{\text{leak}} - \gamma_{\bar{\nu} e}^{\text{leak}}$ is characterized by the leakage timescale t_{leak} so that this equation can be solved explicitly in the hydrodynamic timescale. Then, assuming that the β -equilibrium is achieved, values of the lepton fractions in the β -equilibrium (Y_e^β , $Y_{\nu e}^\beta$, and $Y_{\bar{\nu} e}^\beta$) are calculated from the evolved Y_l .

Second, regarding $Y_{\nu e}^\beta$ and $Y_{\bar{\nu}e}^\beta$ as the maximum allowed values of the neutrino fractions in the next timestep $n + 1$, the source terms are limited so that Y_ν 's in the timestep $n + 1$ cannot exceed $Y_{\nu e}^\beta$'s. Then, the whole of the lepton conservation equations (Eqs. (3.13) – (3.16)) are solved explicitly using these limiters.

Third, the following conditions are checked

$$\mu_p + \mu_e < \mu_n + \mu_{\nu e}, \quad (3.22)$$

$$\mu_n - \mu_e < \mu_p + \mu_{\bar{\nu}e}, \quad (3.23)$$

where μ_p , μ_n , μ_e , $\mu_{\nu e}$ and $\mu_{\bar{\nu}e}$ are the chemical potentials of protons, neutrons, electrons, electron neutrinos, and electron anti-neutrinos, respectively. If both conditions are satisfied, the values of the lepton fractions in the timestep $n + 1$ are set to be those in the β -equilibrium value; Y_e^β , $Y_{\nu e}^\beta$, and $Y_{\bar{\nu}e}^\beta$. On the other hand, if either or both conditions are not satisfied, the lepton fractions in the timestep $n + 1$ is set to be those obtained by solving whole of the lepton-number conservation equations.

A limiter for the evolution of $Y_{\nu x}$ may be also necessary in the case where the pair processes are dominant, for example, in the simulations for collapse of population III stellar core. In this case, the value of $Y_{\nu x}$ at the pair equilibrium (i.e. at $\mu_{\nu x} = 0$), $Y_{\nu x}^{\text{pair}}$ may be used to limit the source term.

3.3. Definition of leakage rates

In this subsection the definitions of the leakage rates Q_α^{leak} and γ_ν^{leak} are presented. Because Q_ν^{leak} may be regarded as the emissivity of neutrinos measured in the *fluid rest frame*, Q_α^{leak} is defined as⁷⁷⁾

$$Q_\alpha^{\text{leak}} = Q_\nu^{\text{leak}} u_\alpha. \quad (3.24)$$

The leakage rates Q_ν^{leak} and γ_ν^{leak} are assumed to satisfy the following properties.

1. The leakage rates approach the local rates Q_ν^{local} and $\gamma_\nu^{\text{local}}$ in the low density, transparent region.
2. The leakage rates approach the diffusion rates Q_ν^{diff} and γ_ν^{diff} in the high density, opaque region.
3. The above two limits should be connected smoothly.

Here, the local rates can be calculated based on the theory of weak interactions and the diffusion rates can be determined based on the diffusion theory (see appendices for the definition of the local and diffusion rates adopted in this paper). There will be several prescriptions to satisfy the requirement (iii).^{63),62)} In this paper, the leakage rates are defined by

$$Q_\nu^{\text{leak}} = (1 - e^{-b\tau_\nu})Q_\nu^{\text{diff}} + e^{-b\tau_\nu}Q_\nu^{\text{local}}, \quad (3.25)$$

$$\gamma_\nu^{\text{leak}} = (1 - e^{-b\tau_\nu})\gamma_\nu^{\text{diff}} + e^{-b\tau_\nu}\gamma_\nu^{\text{local}}, \quad (3.26)$$

where τ_ν is the optical depth of neutrinos and b is a parameter which is typically set as $b^{-1} = 2/3$. The optical depth can be computed from the cross sections in a standard manner.^{63),62)}

In the present implementation, it is not necessary to artificially divide the system into neutrino-trapped and free-streaming regions by the single neutrino-trapping density. Therefore there is no discontinuous boundary which existed in the previous leakage schemes.^{51),52),58)}

As the local production reactions of neutrinos, the electron and positron captures⁶⁶⁾ ($\gamma_{\nu e}^{\text{ec}}$ and $\gamma_{\bar{\nu} e}^{\text{pc}}$), the electron-positron pair annihilation⁷⁸⁾ ($\gamma_{\nu e \bar{\nu} e}^{\text{pair}}$ for electron-type neutrinos and $\gamma_{\nu_x \bar{\nu}_x}^{\text{pair}}$ for the other type), the plasmon decays⁶³⁾ ($\gamma_{\nu e \bar{\nu} e}^{\text{plas}}$ and $\gamma_{\nu_x \bar{\nu}_x}^{\text{plas}}$), and the Bremsstrahlung processes⁷⁹⁾ ($\gamma_{\nu e \bar{\nu} e}^{\text{Brems}}$ and $\gamma_{\nu_x \bar{\nu}_x}^{\text{Brems}}$) are considered in this paper. Then, the local rates for the neutrino fractions are

$$\gamma_{\nu e}^{\text{local}} = \gamma_{\nu e}^{\text{ec}} + \gamma_{\nu e \bar{\nu} e}^{\text{pair}} + \gamma_{\nu e \bar{\nu} e}^{\text{plas}} + \gamma_{\nu e \bar{\nu} e}^{\text{Brems}}, \quad (3.27)$$

$$\gamma_{\bar{\nu} e}^{\text{local}} = \gamma_{\bar{\nu} e}^{\text{pc}} + \gamma_{\nu e \bar{\nu} e}^{\text{pair}} + \gamma_{\nu e \bar{\nu} e}^{\text{plas}} + \gamma_{\nu e \bar{\nu} e}^{\text{Brems}}, \quad (3.28)$$

$$\gamma_{\nu_x}^{\text{local}} = \gamma_{\nu_x \bar{\nu}_x}^{\text{pair}} + \gamma_{\nu_x \bar{\nu}_x}^{\text{plas}} + \gamma_{\nu_x \bar{\nu}_x}^{\text{Brems}}. \quad (3.29)$$

Similarly, the local neutrino energy emission rate Q_{ν}^{local} is given by

$$Q_{\nu}^{\text{local}} = Q_{\nu e}^{\text{ec}} + Q_{\bar{\nu} e}^{\text{pc}} + 2(Q_{\nu e \bar{\nu} e}^{\text{pair}} + Q_{\nu e \bar{\nu} e}^{\text{plas}} + Q_{\nu e \bar{\nu} e}^{\text{Brems}}) \\ + 4(Q_{\nu_x \bar{\nu}_x}^{\text{pair}} + Q_{\nu_x \bar{\nu}_x}^{\text{plas}} + Q_{\nu_x \bar{\nu}_x}^{\text{Brems}}). \quad (3.30)$$

The explicit forms of the local rates in Eqs. (3.27)–(3.30) will be found in Appendices A and B.

We follow the recent work by Rosswog and Liebendörfer⁶²⁾ for the diffusive neutrino emission rates $\gamma_{\nu}^{\text{diff}}$ and Q_{ν}^{diff} in Eqs (3.25) and (3.26). The explicit forms of $\gamma_{\nu}^{\text{diff}}$ and Q_{ν}^{diff} are presented in Appendix C.

§4. Equation of state

In this section we summarize details of EOSs adopted in our current code.

4.1. *Baryons*

In the present version of our code, we employ an EOS by Shen et al.,³⁵⁾ which is derived by the relativistic mean field theory⁸⁰⁾ based on the relativistic Brückner-Hartree-Fock theory.⁸¹⁾ The so-called parameter set TM1⁸⁰⁾ is adopted to reproduce characteristic properties of heavy nuclei. The maximum mass of a cold spherical neutron star in this EOS is much larger than the canonical neutron star mass $\approx 1.4M_{\odot}$ as $\approx 2.2M_{\odot}$.³⁵⁾ The framework of the relativistic mean field theory is extended with the Thomas-Fermi spherical cell model approximation to describe not only the homogeneous matter but also an inhomogeneous one.

The thermodynamical quantities of dense matter at various sets of (ρ, Y_p, T) are calculated to construct the numerical data table for simulation. The table covers a wide range of density $10^{5.1}$ – $10^{15.4}$ g/cm³, electron fraction 0.0–0.56, and temperature 0–100 MeV, which are required for supernova simulation. It should be noted that the causality is guaranteed to be satisfied in this framework, whereas the sound velocity sometimes exceeds the velocity of the light in the non-relativistic framework, e.g., in the EOS by Lattimer and Swesty.⁸²⁾ This is one of the benefits of the relativistic EOS.

Although we employ the nuclear EOS by Shen et al. in this work, it is easy to replace the EOS. In the future we plan to implement other EOSs such as a hyperonic matter EOS.⁸³⁾

Because the table of the original EOS by Shen et al. does not include the thermodynamical quantities of the leptons (electrons, positrons, and neutrinos if necessary) and photons, one has to consistently include them to the table.

4.2. Electrons and Positrons

To consistently calculate the pressure and the internal energy of the electron and positron, the charge neutrality condition $Y_p = Y_e$ should be solved to determine the electron chemical potential μ_e for each value of the baryon rest-mass density ρ and the temperature T in the EOS table. Namely, it is required to solve the equation

$$n_e(\mu_e, T) \equiv n_- - n_+ = \frac{\rho Y_e}{m_u} \quad (4.1)$$

in terms of μ_e for given values of ρ , T , and Y_e ($= Y_p$). Here, $m_u = 931.49432$ MeV is the atomic mass unit, and n_- and n_+ are the total number densities (i.e., including the electron-positron pair) of the electrons and positrons, respectively.

Assuming that the electrons obey the Fermi-Dirac distribution (which is derived under the assumption of thermodynamic equilibrium), the number density (n_-), the pressure (P_-), and the internal energy density (u_-) of the electron are written as⁸⁴⁾

$$n_- = \frac{1}{\pi^2 \hbar^3} \int_0^\infty \frac{p^2 dp}{\exp[-\eta_e + \tilde{\epsilon}/k_B T] + 1}, \quad (4.2)$$

$$P_- = \frac{1}{\pi^2 \hbar^3} \int_0^\infty \frac{p^3 (\partial \tilde{\epsilon} / \partial p) dp}{\exp[-\eta_e + \tilde{\epsilon}/k_B T] + 1}, \quad (4.3)$$

$$u_- = \frac{1}{\pi^2 \hbar^3} \int_0^\infty \frac{p^2 \tilde{\epsilon} dp}{\exp[-\eta_e + \tilde{\epsilon}/k_B T] + 1}. \quad (4.4)$$

Here \hbar , k_B , and $\eta_e \equiv \mu_e/k_B T$ are the Planck's constant, the Boltzmann's constant and the so-called degeneracy parameter. $\tilde{\epsilon}(p) = \sqrt{m_e^2 c^4 + p^2} - m_e c^2$ is the kinetic energy of a free electron. If we choose the zero point of our energy scale for electrons at $\tilde{\epsilon} = 0$, we have to assign a total energy of $\tilde{\epsilon}_+ = \sqrt{m_e^2 c^4 + p^2} + m_e c^2$ to a free positron.⁸⁴⁾ Thus the number density (n_+), the pressure (P_+), and the internal energy density (u_+) of positrons are given by⁸⁴⁾

$$n_+ = \frac{1}{\pi^2 \hbar^3} \int_0^\infty \frac{p^2 dp}{\exp[-\eta_+ + \tilde{\epsilon}_+/k_B T] + 1}, \quad (4.5)$$

$$P_+ = \frac{1}{\pi^2 \hbar^3} \int_0^\infty \frac{p^3 (\partial \tilde{\epsilon}_+ / \partial p) dp}{\exp[-\eta_+ + \tilde{\epsilon}_+/k_B T] + 1}, \quad (4.6)$$

$$u_+ = \frac{1}{\pi^2 \hbar^3} \int_0^\infty \frac{p^2 (\tilde{\epsilon} + 2m_e c^2) dp}{\exp[-\eta_+ + \tilde{\epsilon}_+/k_B T] + 1}, \quad (4.7)$$

where $\eta_+ = -\eta_e$ is the degeneracy parameter of the positrons.

4.3. Photons

The pressure and the specific internal energy density of photons are given by

$$P_r = \frac{a_r T^4}{3}, \quad \varepsilon_r = \frac{a_r T^4}{\rho}, \quad (4.8)$$

where a_r is the radiation constant $a_r = (\pi^2 k_B^4)/(15c^3 \hbar^3)$ and c is the velocity of light.

4.4. Trapped neutrinos

In this paper, the trapped-neutrinos are assumed to interact sufficiently frequently with matter that be thermalized. Therefore they are described as ideal Fermi gases with the matter temperature. Then, from the neutrino fractions Y_ν , the chemical potentials of neutrinos are calculated by solving

$$Y_\nu = Y_\nu(\mu_\nu, T). \quad (4.9)$$

Using the chemical potentials, μ_ν , and the matter temperature, the pressure and the internal energy of the trapped-neutrinos are calculated in the same manner as for electrons.

4.5. The sound velocity

In the high-resolution shock-capturing scheme for hydrodynamics, we in general need to evaluate the sound velocity c_s ,

$$c_s^2 = \frac{1}{h} \left[\frac{\partial P}{\partial \rho} \Big|_\epsilon + \frac{P}{\rho} \frac{\partial P}{\partial \epsilon} \Big|_\rho \right]. \quad (4.10)$$

The derivatives of the pressure are calculated by

$$\frac{\partial P}{\partial \rho} \Big|_\epsilon = \sum_{i=B,e,r,\nu} \left[\frac{\partial P_i}{\partial \rho} \Big|_T - \frac{\partial P_i}{\partial T} \Big|_\rho \left(\sum_{j=B,e,r,\nu} \frac{\partial \epsilon_j}{\partial \rho} \Big|_T \right) \left(\sum_{k=B,e,r,\nu} \frac{\partial \epsilon_k}{\partial T} \Big|_\rho \right)^{-1} \right] \quad (4.11)$$

$$\frac{\partial P}{\partial \epsilon} \Big|_\rho = \left(\sum_{i=B,e,r,\nu} \frac{\partial P_i}{\partial T} \Big|_\rho \right) \left(\sum_{j=B,e,r,\nu} \frac{\partial \epsilon_j}{\partial T} \Big|_\rho \right)^{-1}, \quad (4.12)$$

where 'B', 'e', 'ph' and ' ν ' in the sum denote the baryon, electron, photons, and neutrino quantities.

The derivatives for the baryon parts are evaluated by taking a finite difference of the table data. On the other hand, the derivatives for the electron parts can be evaluated semi-analytically. Because there are in general the phase transition regions in an EOS table for baryons and moreover the EOS may contain some non-smooth spiky structures, careful treatments are necessary when evaluating the derivatives of thermodynamical quantities. In the present EOS table, the derivatives are carefully evaluated so that there are no spiky behaviors in the resulting sound velocities.

§5. Basic equations and Numerical methods

5.1. Einstein's equation and gauge conditions

The standard variables in the 3+1 decomposition are the three-dimensional metric γ_{ij} and the extrinsic curvature K_{ij} on the three-dimensional hypersurface⁸⁵⁾ defined by

$$\gamma_{\mu\nu} \equiv g_{\mu\nu} + n_\mu n_\nu, \quad (5.1)$$

$$K_{\mu\nu} \equiv -\frac{1}{2}\mathcal{L}_n \gamma_{\mu\nu}, \quad (5.2)$$

where $g_{\mu\nu}$ is the spacetime metric, n_μ is the unit normal to a three-dimensional hypersurface, and \mathcal{L}_n is the Lie derivative with respect to the unit normal n^μ . Then we can write the line element in the form

$$ds^2 = -\alpha^2 dt^2 + \gamma_{ij}(dx^i + \beta^i dt)(dx^j + \beta^j dt), \quad (5.3)$$

where α and β^i are the lapse function and the shift vector which describe the gauge degree of freedom.

In the BSSN reformulation,^{86),87)} the spatial metric γ_{ij} is conformally decomposed as $\gamma_{ij} = e^{4\phi}\tilde{\gamma}_{ij}$ where the condition $\det(\tilde{\gamma}_{ij}) = 1$ is imposed for the conformal metric $\tilde{\gamma}_{ij}$. From this condition, the conformal factor is written as $\phi = \frac{1}{12}\ln\gamma$ and $\gamma \equiv \det(\gamma_{ij})$. The extrinsic curvature K_{ij} is decomposed into the trace part K and the traceless part A_{ij} as $K_{ij} = A_{ij} + (1/3)\gamma_{ij}K$. The traceless part A_{ij} is conformally decomposed as $A_{ij} = e^{4\phi}\tilde{A}_{ij}$. Thus the fundamental quantities for the evolution equation are now split into ϕ , $\tilde{\gamma}_{ij}$, K , and \tilde{A}_{ij} . Furthermore, the auxiliary variable $F_i \equiv \delta^{jk}\partial_k\tilde{\gamma}_{ij}$ is introduced in the BSSN reformulation.⁸⁶⁾

The basic equations to be solved are

$$\left(\partial_t - \beta^k\partial_k\right)\phi = \frac{1}{6}\left(-\alpha K + \partial_k\beta^k\right), \quad (5.4)$$

$$\left(\partial_t - \beta^k\partial_k\right)\tilde{\gamma}_{ij} = -2\alpha\tilde{A}_{ij} + \tilde{\gamma}_{ik}\partial_j\beta^k + \tilde{\gamma}_{jk}\partial_i\beta^k - \frac{2}{3}\tilde{\gamma}_{ij}\partial_k\beta^k, \quad (5.5)$$

$$\left(\partial_t - \beta^k\partial_k\right)K = -D^k D_k\alpha + \alpha\left[\tilde{A}_{ij}\tilde{A}^{ij} + \frac{1}{3}K^2\right] + 4\pi\alpha(\rho_h + S), \quad (5.6)$$

$$\begin{aligned} \left(\partial_t - \beta^k\partial_k\right)\tilde{A}_{ij} = e^{-4\phi}\left[\alpha\left(R_{ij} - \frac{1}{3}e^{4\phi}\tilde{\gamma}_{ij}R\right) - \left(D_i D_j\alpha - \frac{1}{3}e^{4\phi}\tilde{\gamma}_{ij}D^k D_k\alpha\right)\right] \\ + \alpha\left(K\tilde{A}_{ij} - 2\tilde{A}_{ik}\tilde{A}^k{}_j\right) + \tilde{A}_{ik}\partial_j\beta^k + \tilde{A}_{jk}\partial_i\beta^k - \frac{2}{3}\tilde{A}_{ij}\partial_k\beta^k \\ - 8\pi\alpha\left(e^{-4\phi}S_{ij} - \frac{1}{3}\tilde{\gamma}_{ij}S\right), \end{aligned} \quad (5.7)$$

$$\begin{aligned} \left(\partial_t - \beta^k\partial_k\right)F_i = -16\pi\alpha j_i \\ + 2\alpha\left\{f^{kj}\partial_j\tilde{A}_{ik} + \tilde{A}_{ik}\partial_j f^{kj} - \frac{1}{2}\tilde{A}^{jl}\partial_i h_{jl} + 6\tilde{A}^k{}_i\partial_k\phi - \frac{2}{3}\partial_i K\right\} \\ + \delta^{jk}\left\{-2\tilde{A}_{ij}\partial_k\alpha + \left(\partial_k\beta^l\right)\partial_l h_{ij}\right\} \end{aligned}$$

$$+\partial_k \left(\tilde{\gamma}_{il} \partial_j \beta^l + \tilde{\gamma}_{jl} \partial_i \beta^l - \frac{2}{3} \tilde{\gamma}_{ij} \partial_l \beta^l \right) \Big\}, \quad (5.8)$$

where ${}^{(3)}R$, ${}^{(3)}R_{ij}$, and D_i are the Ricci scalar, the Ricci tensor, and the covariant derivative associated with three-dimensional metric γ_{ij} , respectively. The matter source terms, $\rho_h \equiv (T^{\text{Total}})^{\alpha\beta} n_\alpha n_\beta$, $j_i \equiv -(T^{\text{Total}})^{\alpha\beta} \gamma_{i\alpha} n_\beta$, and $S_{ij} \equiv (T^{\text{Total}})^{\alpha\beta} \gamma_{i\alpha} \gamma_{j\beta}$, are the projections of the stress-energy tensor with respect to n^μ and $\gamma_{\mu\nu}$, and $S \equiv \gamma_{ij} S^{ij}$.

We assume the axial symmetry of the spacetime and the so-called Cartoon method^{(88), (89)} is adopted to avoid problems around the coordinate singularities of the cylindrical coordinates. Except for this, the numerical schemes for solving the Einstein's equation are essentially the same as those in Ref. 90). We use 4th-order finite difference scheme in the spatial direction and the 3rd-order Runge-Kutta scheme in the time integration. The advection terms such as $\beta^i \partial_i \phi$ are evaluated by a 4th-order upwind scheme.

As the gauge conditions for the lapse, we use the so-called 1 + log slicing:⁽⁹¹⁾

$$(\partial_t - \mathcal{L}_\beta)\alpha = -2K\alpha. \quad (5.9)$$

It is known that the 1 + log slicing enables to perform a long term evolution of neutron stars as well as has strong singularity avoidance properties in the black hole spacetime.

The shift vector is determined by solving the following dynamical equation⁽⁹²⁾

$$\partial_t \beta^k = \tilde{\gamma}^{kl} (F_l + \Delta t \partial_t F_l). \quad (5.10)$$

Here the second term in the right-hand side is necessary for numerical stability.⁽⁹²⁾

5.2. The hydrodynamic equations in leakage scheme

The basic equations for general relativistic hydrodynamics in our leakage scheme are the continuity equation, the lepton-number conservation equations, and the local conservation equation of the energy-momentum. We assume the axial symmetry of the spacetime and the hydrodynamics equations are solved in the cylindrical coordinates (ϖ, φ, z) where $\varpi = \sqrt{x^2 + y^2}$. In the axisymmetric case, the hydrodynamics equations should be written in the cylindrical coordinate. On the other hand, in the Cartoon method,^{(88), (89)} Einstein's equation are solved in the $y = 0$ plane for which $x = \varpi$, $u_\varpi = u_x$, $u_\varphi = x u_y$, and the other similar relations hold for vector and tensor quantities. Taking into these facts, the hydrodynamic equations may be written using the Cartesian coordinates replacing (ϖ, φ) by (x, y) . In the following, we write down explicit forms of the equations for the purpose of convenience. Numerical tests for basic parts of the code of solving the hydrodynamics equations are extensively performed in Ref. 89). The equations are solved using the third-order high-resolution central scheme of Kurganov and Tadmor.^{(93), (61)}

5.2.1. The Continuity and lepton-number conservation equations

The continuity equation for the baryon rest mass is

$$\nabla_\alpha (\rho u^\alpha) = 0. \quad (5.11)$$

As fundamental variables for numerical simulations, the following quantities are introduced: $\rho_* \equiv \rho w e^{6\phi}$ and $v^i \equiv u^i/u^t$ where $w \equiv \alpha u^t$. Then, the continuity equation is written as

$$\partial_t(\rho_*) + \frac{1}{x}\partial_x(\rho_*v^x) + \partial_z(\rho_*v^z) = 0. \quad (5.12)$$

Using the continuity equation, the lepton-number conservation equations (3.13) – (3.16) are written as

$$\partial_t(\rho_*Y_L) + \frac{1}{x}\partial_x(\rho_*Y_Lv^x) + \partial_z(\rho_*Y_Lv^z) = \rho_*\gamma_L, \quad (5.13)$$

where Y_L and γ_L are abbreviated expressions of the lepton fractions and the source terms.

5.2.2. Energy-momentum conservation

As fundamental variables for numerical simulations, we define the quantities $\hat{u}_i \equiv hu_i$ and $\hat{e} \equiv hw - P(\rho w)^{-1}$. Then, the Euler equation $\gamma_i^\alpha \nabla_\beta T_\alpha^\beta = -\gamma_i^\alpha Q_\alpha^{\text{leak}}$, and the energy equation $n^\alpha \nabla_\beta T_\beta^\alpha = -n^\alpha Q_\alpha^{\text{leak}}$ can be written as

$$\begin{aligned} \partial_t(\rho_*\hat{u}_A) + \frac{1}{x}\partial_x \left[x \left\{ \rho_*\hat{u}_A v^x + P\alpha e^{6\phi} \delta_A^x \right\} \right] + \partial_z \left[\rho_*\hat{u}_A v^z + P\alpha e^{6\phi} \delta_A^z \right] \\ = -\rho_* \left[wh\partial_A\alpha - \hat{u}_i\partial_A\beta^i + \frac{\alpha e^{-4\phi}}{2wh}\hat{u}_k\hat{u}_l\partial_A\tilde{\gamma}^{kl} - \frac{2\alpha h(w^2-1)}{w}\partial_A\phi \right] \\ + P\partial_A(\alpha e^{6\phi}) + \frac{(\rho_*u_yv^y + P\alpha e^{6\phi})\delta_A^x}{x} - \alpha e^{6\phi}Q_A^{\text{leak}}, \end{aligned} \quad (5.14)$$

$$\partial_t(\rho_*\hat{u}_y) + \frac{1}{x^2}\partial_x(x^2\rho_*\hat{u}_yv^y) + \partial_z(\rho_*\hat{u}_yv^z) = -\alpha e^{6\phi}Q_y^{\text{leak}}, \quad (5.15)$$

$$\begin{aligned} \partial_t(\rho_*\hat{e}) + \frac{1}{x}\partial_x \left[x \left\{ \rho_*v^x\hat{e} + P e^{6\phi}(v^x + \beta^x) \right\} \right] + \partial_z \left[\rho_*v^z\hat{e} + P e^{6\phi}(v^z + \beta^z) \right] \\ = \alpha e^{6\phi}PK + \frac{\rho_*}{u^th}\hat{u}_k\hat{u}_lK^{kl} - \rho_*\hat{u}_i\gamma^{ij}D_j\alpha - \alpha e^{6\phi}Q_\alpha^{\text{leak}}n^\alpha, \end{aligned} \quad (5.16)$$

where the subscript A denotes x or z component.

The evolution equation of streaming-neutrinos $\nabla_\beta(T^{\nu,S})_\alpha^\beta = Q_\alpha^{\text{leak}}$ gives

$$\begin{aligned} \partial_t(\hat{E}) + \frac{1}{x}\partial_x \left[x(\alpha\hat{F}^x - \beta^x\hat{E}) \right] + \partial_z \left[(\alpha\hat{F}^z - \beta^z\hat{E}) \right] \\ = \frac{\alpha\hat{E}K}{3} - \hat{F}^k\partial_k\alpha + \alpha e^{6\phi}Q_a^{\text{leak}}n^a, \end{aligned} \quad (5.17)$$

$$\begin{aligned} \partial_t(\hat{F}_A) + \frac{1}{x}\partial_x \left[x \left(\frac{1}{3}\alpha\hat{E}\delta_A^x - \beta^x\hat{F}_A \right) \right] + \partial_z \left[\left(\frac{1}{3}\alpha\hat{E}\delta_A^z - \beta^z\hat{F}_A \right) \right] \\ = -\hat{E}\partial_A\alpha + \hat{F}_k\partial_A\beta^k + 2\alpha\hat{E}\partial_A\phi + \frac{(\hat{E}/3 - \hat{F}_y\beta^y)\delta_A^x}{x} + \alpha e^{6\phi}Q_A^{\text{leak}}, \end{aligned} \quad (5.18)$$

$$\partial_t(\hat{F}_y) - \frac{1}{x^2}\partial_x \left[x^2\beta^x\hat{F}_y \right] - \partial_z \left[\beta^z\hat{F}_y \right] = \alpha e^{6\phi}Q_y^{\text{leak}}, \quad (5.19)$$

where $\hat{E} = e^{6\phi}E$ and $\hat{F}_i = e^{6\phi}F_i$, and the subscript A again denotes x or z component. The closure relation $P_{\alpha\beta} = E\gamma_{\alpha\beta}/3$ is also substituted.

5.3. Recover of $(\rho, Y_e/Y_l, T)$

The quantities numerically evolved in the relativistic hydrodynamics are the conserved quantities $(\rho_*, \hat{u}_i, \hat{e})$ and the lepton fraction Y_e or Y_l . The argument variables, $(\rho, (Y_e \text{ or } Y_l), T)$, of the EOS table, together with the weight factor $w = \sqrt{1 + \gamma^{ij} u_i u_j}$, should be calculated from the conserved quantities at each time slice. Note that the electron (Y_e) or lepton fraction (Y_l) is readily given by numerical evolution at each time slice whereas ρ , u_i , and T are not. This fact requires us to find an efficient method for determining w .

5.3.1. Non- β -equilibrium case

In the case that the β -equilibrium condition is not satisfied, the argument quantities (ρ, Y_e, T) can be reconstructed from the conserved quantities in the following straightforward manner.

1. Give a trial value of w , referred to as \tilde{w} . Then, one obtains a trial value of the rest mass density from $\tilde{\rho} = \rho_*/(\tilde{w}e^{6\phi})$.
2. A trial value of the temperature, \tilde{T} , can be obtained by solving the following equation:

$$\hat{e} = \left(1 + \tilde{\varepsilon} + \frac{\tilde{P}}{\tilde{\rho}}\right) \tilde{w} - \frac{\tilde{P}}{\tilde{\rho}\tilde{w}} \equiv \tilde{e}(\tilde{\rho}, Y_e, \tilde{T}). \quad (5.20)$$

Here, one dimensional search over the EOS table is required to obtain \tilde{T} .

3. The next trial value of w is given by $\tilde{w} = \sqrt{1 + e^{-4\phi} \tilde{\gamma}^{ij} \hat{u}_i \hat{u}_j \tilde{h}^{-2}}$, where the specific enthalpy was calculated as $\tilde{h} = \tilde{h}(\tilde{\rho}, Y_e, \tilde{T})$ in the step 2.
4. Repeat the procedures (1)–(3) until a required degree of convergence is achieved. Convergent solutions of the temperature and w are obtained typically in 10 iterations.

5.3.2. The β -equilibrium case

On the other hand, in the case that the β -equilibrium condition is satisfied, one has to reconstruct the argument quantities (ρ, Y_e, T) from the conserved quantities and Y_l , under the assumption of the β -equilibrium. In this case, two-dimensional recover $(Y_l, \hat{e}) \implies (Y_e, T)$ would be required for a given value of \tilde{w} . A serious problem is that in this case, there may be more than one combination of (Y_e, T) which gives the same values of Y_l and \hat{e} . Therefore, we have to adopt a different method to recover (ρ, Y_e, T) . Under the assumption of the β -equilibrium, the electron fraction is related to the total lepton fraction: $Y_e = Y_e(\rho, Y_l, T)$. Using this relation, the EOS table can be rewritten in terms of the argument variables of (ρ, Y_l, T) . Then, the same strategy as in the non- β -equilibrium case can be adopted. Namely,

1. Give a trial value \tilde{w} . Then one obtains a trial value of the rest mass density.
2. A trial value of the temperature can be obtained by solving $\hat{e} = \tilde{e}(\tilde{\rho}, Y_l, \tilde{T})$, with one dimensional search over the EOS table.
3. The next trial value of w is given by $\tilde{w} = \sqrt{1 + e^{-4\phi} \tilde{\gamma}^{ij} \hat{u}_i \hat{u}_j \tilde{h}^{-2}}$.
4. Repeat the procedures (1)–(3) until a required degree of convergence is achieved. The electron fraction is given as $Y_e = Y_e(\rho, Y_l, T)$ in the (new) EOS table.

Model		$\Phi_c \leq 0.0125$	$\leq \Phi_c \leq 0.025$	$\leq \Phi_c \leq 0.05$	$\leq \Phi_c \leq 0.1$	$\Phi_c \geq 0.1$
S15	Δx_0	3.26	1.60	0.820	0.414	0.217
	δ	0.002	0.002	0.002	0.002	0.002
	N	444	668	924	1212	1532
	L (km)	2330	2239	2188	2124	2103
S15 (low)	Δx_0	5.10	2.90	1.44	0.760	0.396
	δ	0.002	0.00215	0.0023	0.00245	0.0026
	N	316	444	636	828	1020
	L (km)	2244	2151	2073	2043	2000

Table I. Summary of the regridding procedure. The values of the minimum grid spacing Δx_0 (in units of km), the non-uniform-grid factor δ , and the grid number N for each range of $\Phi_c = 1 - \alpha_c$ are listed.

In the case of a simplified or analytic EOS, the Newton-Raphson method may be applied to recover the primitive variables. In the case of a tabulated EOS, by contrast, the Newton-Raphson method may not be a good approach because it requires derivatives of thermodynamical quantities which in general cannot be calculated precisely from a tabulated EOS by the finite differentiating method.

5.4. Grid Setting

In numerical simulations, we adopt a nonuniform grid, in which the grid spacing is increased as

$$dx_{j+1} = (1 + \delta)dx_j, \quad dz_{l+1} = (1 + \delta)dz_l \quad (5.21)$$

where $dx_j \equiv x_{j+1} - x_j$, $dz_l \equiv z_{l+1} - z_l$, and δ is a constant. In addition, a regridding technique^{47),30)} is adopted to assign a sufficiently large number of grid points inside the collapsing core, saving the CPU time efficiently. The regridding is carried out whenever the characteristic radius of the collapsing star decreases by a factor of a 2–3. At each regridding, the minimum grid spacing is decreased by a factor of ~ 2 while the geometrical factor δ is unchanged (see Table I).

All the quantities on the new grid are calculated using the fifth-order Lagrange interpolation. To avoid discarding the matter in the outer region, we also increase the grid number at each regridding. For the regridding, we define a relativistic gravitational potential $\Phi_c \equiv 1 - \alpha_c$ ($\Phi_c > 0$) where α_c is the central value of the lapse function. Because Φ_c is approximately proportional to M/R where M and R are characteristic mass and radius of the core, Φ_c^{-1} can be used as a measure of the characteristic length scale of the stellar core for the regridding. In Table I, we summarize the regridding parameters of each level of the grid.

§6. Results

As a test problem, we perform a collapse simulation of spherical presupernova core and compare the results with those in the previous studies, to see the validity of the present code. Most of the following results are not novel astrophysically, but are novel in the sense that stellar core collapse can be followed by a *multidimensional fully general relativistic simulation taking account of microphysical processes*. In

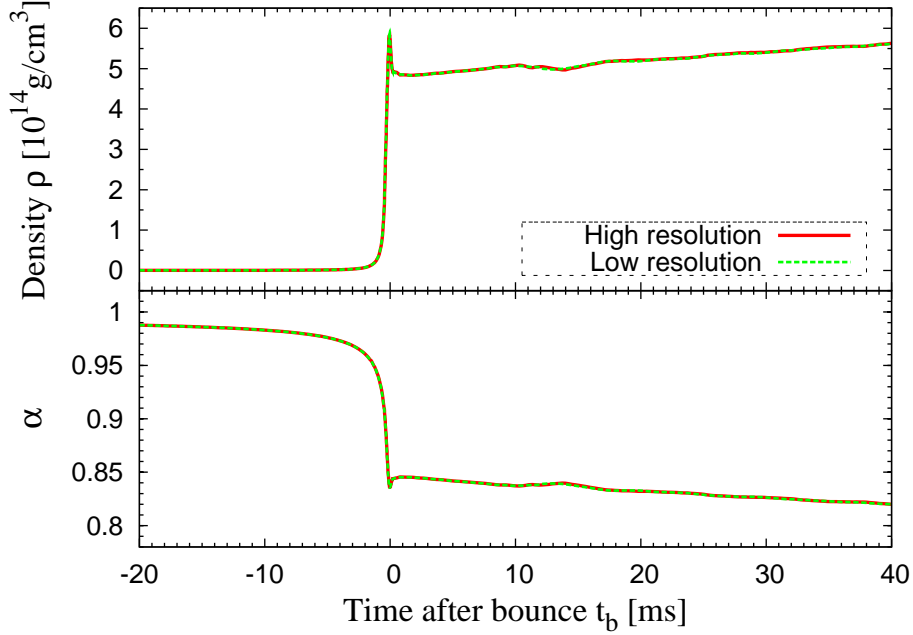


Fig. 1. Evolution of the central density ρ_c (upper panel) and the central value of the lapse function α_c (lower panel). The solid curves are results for the finer grid resolution and the dotted curves are results of the coarser grid resolution.

§ 6.2, § 6.3, and § 6.4, we first review the basic features of the collapse dynamics and the shock formation, the stall of shock, and convective activities. Then we compare our results with those in the previous studies in § 6.5.

6.1. Initial condition

In this paper, we adopt a recent presupernova model of massive star by Woosley, Heger, and Weaver:⁹⁴⁾ $15M_{\odot}$ model with solar metallicity (hereafter S15 model). We follow the dynamical evolution of the central part which constitutes the Fe core and the inner part of the Si-shell. We read in the density, the electron fraction, the temperature and the velocity (v_i) of the original initial data and derive other thermodynamical quantities using the EOS table.

Note that the procedure of remapping the original initial data into the grid adopted in the numerical simulations is coordinate-dependent in general relativity. In this paper, we read in the original data *as a function of the coordinate radius*. In this case, the baryon rest-mass of the core is slightly larger than the original one, because it is defined by

$$M_* = \int \rho_* dx^3 = \int \rho (we^{6\phi}) d^3x, \quad (6.1)$$

where $we^{6\phi} > 1$.

6.2. Core bounce and shock formation

Figure 1 displays the time evolution of the central rest-mass density ρ and the central value of the lapse function. This figure shows that the stellar core collapse to a neutron star can be divided into three phases; the infall phase, the bounce phase, and the quasi-static evolution phase (see Refs. 21) and 24) for the case of rotational collapse). The general feature of the collapse is as follows.

The infall phase sets in due to gravitational instability of the iron core triggered by the sudden softening of the EOS, which is associated primarily with the electron capture and partially with the photo-dissociation of the heavy nuclei. The collapse in an early phase proceeds almost homologously. However, the collapse in the central region is accelerated with time because the electron capture reduces the degenerate pressure of electrons which provides the main part of the total pressure. Furthermore, the neutrino emission associated with the electron capture reduces the thermal pressure of the core. Here the inner part of the core, which collapses nearly homologously with a subsonic infall velocity, constitutes the inner core. On the other hand, the outer region in which the infall velocity is supersonic constitutes the outer core.

The collapse proceeds until the central part of the iron core reaches the nuclear density ($\sim 2 \times 10^{14}$ g/cm³), and then, the inner core experiences the bounce. Because of its large inertia and large kinetic energy induced by the infall, the inner core overshoots its hypothetical equilibrium state. The stored internal energy of the inner core at the maximum compression is released through strong pressure waves generated inside the inner core. The pressure waves propagate from the center to the outer region until they reach the sonic point located at the edge of the inner core. Because the sound cones tilt inward beyond the sonic point, the pressure disturbance cannot propagate further and forms a shock just inside the sonic point. A shock wave is formed at the edge of the inner core and propagates outward.

After this phase, the proto-neutron star experiences the quasi-static evolution phase. In this phase, the central value of density (the lapse function) increases (decreases) gradually, because the matter in the outer region falls into the proto-neutron star and because neutrinos are emitted carrying away the energy and lepton-number from the proto-neutron star.

Figure 2 shows the radial profiles in the equator of the lepton fractions at the bounce. The central values of the electron, the electron-neutrinos, and the total-lepton fractions are ≈ 0.32 , 0.05, and 0.37, respectively. The electron-anti-neutrino fraction is almost zero through out the core because only very small amount of positrons exist due to the high degree of electron degeneracy.

6.3. Neutrino bursts and stall of shock

As the shock wave propagates outward, the kinetic energy of the infall matter is converted into the thermal energy behind the shock. The conversion rate of infall kinetic energy may be estimated approximately as

$$L_{\text{heat}} \sim 4\pi R_s^2 (\rho_{\text{infall}} v_{\text{infall}}^3 / 2)$$

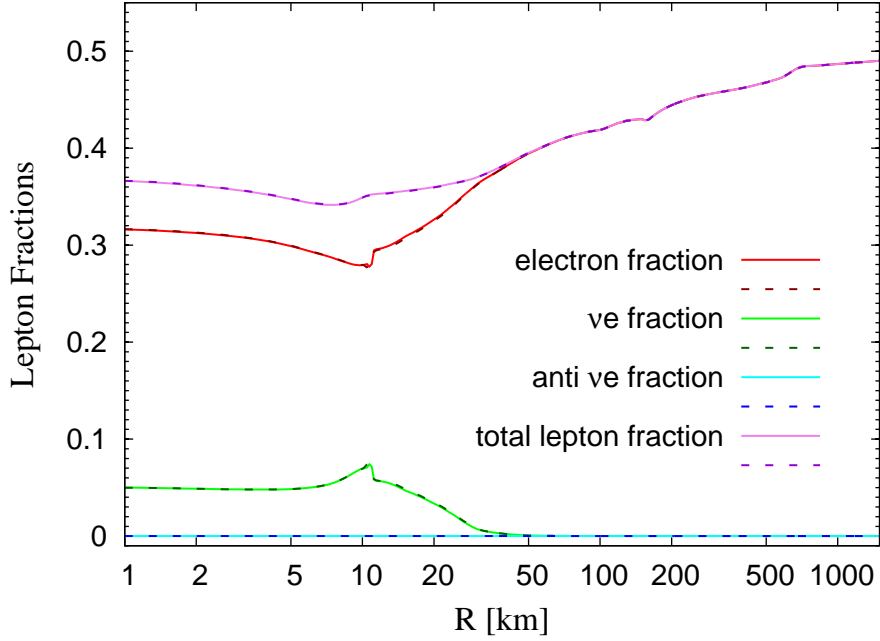


Fig. 2. The radial profiles of the electron, ν_{e^-} , $\bar{\nu}_{e^-}$, and the total lepton fraction at the bounce. The results for the finer grid resolution (solid curve) and for the coarser grid resolution (the dotted curves) are shown together. The two results are almost identical.

$$\sim 1.4 \times 10^{53} \text{ ergs/s} \left(\frac{R_s}{100 \text{ km}} \right)^2 \left(\frac{\rho_{\text{infall}}}{10^9 \text{ g/cm}^3} \right) \left(\frac{v_{\text{infall}}}{0.2c} \right)^3, \quad (6.2)$$

where R_s and ρ_{infall} are radius of the shock wave and the density of infall matter, and we here recover the velocity of the light (c). Here, we assume that all the kinetic energy is converted to the thermal energy.

At the same time, the shock wave suffers from the energy loss by the photo-dissociation of the iron to α -particles and free nucleons. The fraction of this energy loss is⁹⁵⁾

$$\epsilon_{\text{diss}} \sim 1.5 \times 10^{51} \text{ ergs per } 0.1M_{\odot}. \quad (6.3)$$

Thus, the energy loss rate due to the photo-dissociation is

$$L_{\text{diss}} \sim \dot{M}_{\text{shock}} \epsilon_{\text{diss}} \sim 1.1 \times 10^{53} \text{ ergs/s} \left(\frac{R_s}{100 \text{ km}} \right)^2 \left(\frac{\rho_{\text{infall}}}{10^9 \text{ g/cm}^3} \right) \left(\frac{v_{\text{infall}}}{0.2c} \right), \quad (6.4)$$

where $\dot{M}_{\text{shock}} \sim 4\pi R_s^2 \rho_{\text{infall}} v_{\text{infall}}$ is mass-accretion rate to the shock front.

The ratio of L_{heat} to L_{diss} is

$$\frac{L_{\text{heat}}}{L_{\text{diss}}} \approx 1.2 \left(\frac{v_{\text{infall}}}{0.2c} \right)^2. \quad (6.5)$$

Therefore the energy loss rate by the photo-dissociation will eventually overcome the hydrodynamic power, because the infall velocity, which is $\approx (GM_{\text{ic}}/R_s)^{1/2}$, decreases as the shock wave propagates outward.

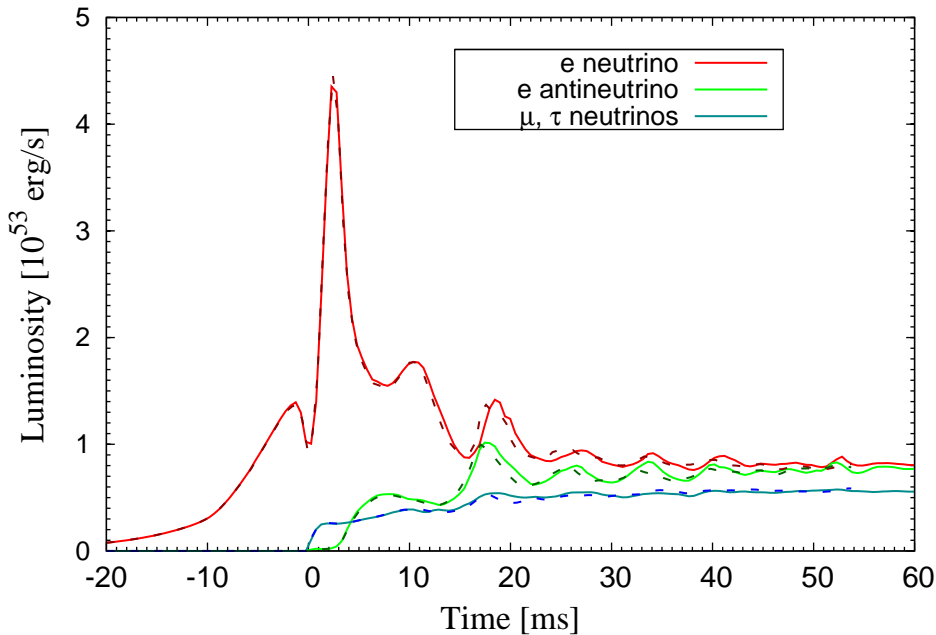


Fig. 3. Time evolution of the neutrino luminosities. The results in the finer grid resolution (solid curves) and in the coarser grid resolution (dashed curves) are shown together. The two results are approximately identical until the convective phase sets in, whereas small disagreement is found in the convective phase.

Furthermore, when the shock wave crosses the neutrino-sphere, spiky burst emissions of neutrinos, the so-called neutrino bursts, occur: Neutrinos in the hot post-shock region are copiously emitted without interacting core matter. Figure 3 shows the neutrino luminosity as a function of time calculated by^(61),77)

$$L_\nu = \int \alpha e^{6\phi} u_t \dot{Q}_\nu d^3x. \quad (6-6)$$

The peak luminosity is $L_{\nu_e} \approx 4.5 \times 10^{53}$ ergs/s. This neutrino burst significantly reduces the thermal energy of the shock. Consequently, the shock wave stalls at ≈ 80 km soon after the neutrino burst. The peak luminosity and the shock-stall radius agree approximately with the previous one-dimensional fully general relativistic study.⁹⁶⁾

When the shock wave stalls, negative gradients of the entropy per baryon and the total-lepton (electron) fraction appear because neutrinos carry away both the energy and the lepton number. Figure 4 shows the radial profiles of the infall velocity, the density, the entropy per baryon, and the total lepton fraction in the equator. This figure clearly shows that negative gradients of the entropy per baryon and the total lepton fraction are formed above the neutrino sphere. As we shall see in § 6.4, such configurations are known to be unstable to convection, which is known to as the proto-neutron star convection.

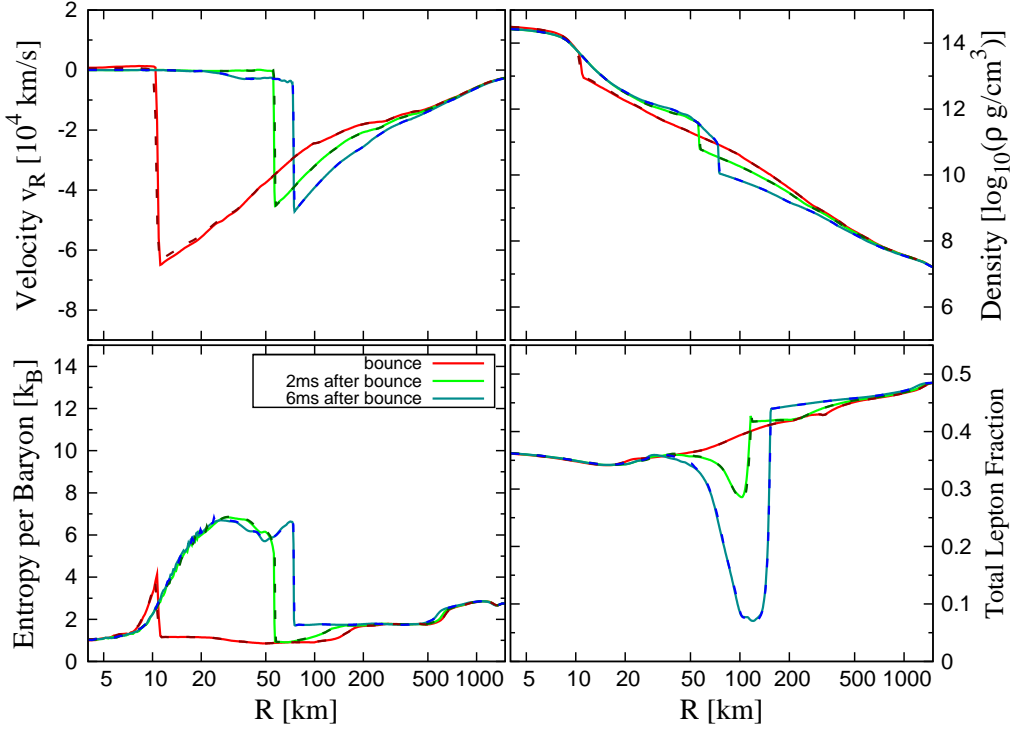


Fig. 4. The radial profiles of the infall velocity, the density, the entropy per baryon, and the total lepton fraction at bounce, at 2 ms and 6ms after bounce. The results for the finer grid resolution (solid curves) and for the coarser grid resolution (the dotted curves) are shown together and they are shown to be approximately identical.

6.4. Convective activities

Let us investigate the stability of the envelope of the proto-neutron star following Lattimer and Mazurek.⁹⁷⁾ We consider the following parameter

$$N^2 \equiv \frac{g_{\text{eff}}}{\rho} \left[\left(\frac{d\rho}{dr} \right)_{\text{amb}} - \left(\frac{d\rho}{dr} \right)_{\text{blob}} \right], \quad (6.7)$$

where g_{eff} is the effective gravitational acceleration defined to be positive in the negative radial direction, the subscript 'amb' refers to the ambient core structure, and 'blob' denotes the blob element which is under an isolated displacement. The condition $N^2 < 0$ implies that the structure is unstable to convective overturn (e.g. Ref. 97)).

Assuming that the fluid elements maintain the pressure equilibrium with its surroundings, we have

$$\left(\frac{d\rho}{dr} \right)_{\text{blob}} = \left(\frac{d\rho}{dP} \right)_{\text{blob}} \left(\frac{dP}{dr} \right)_{\text{amb}}. \quad (6.8)$$

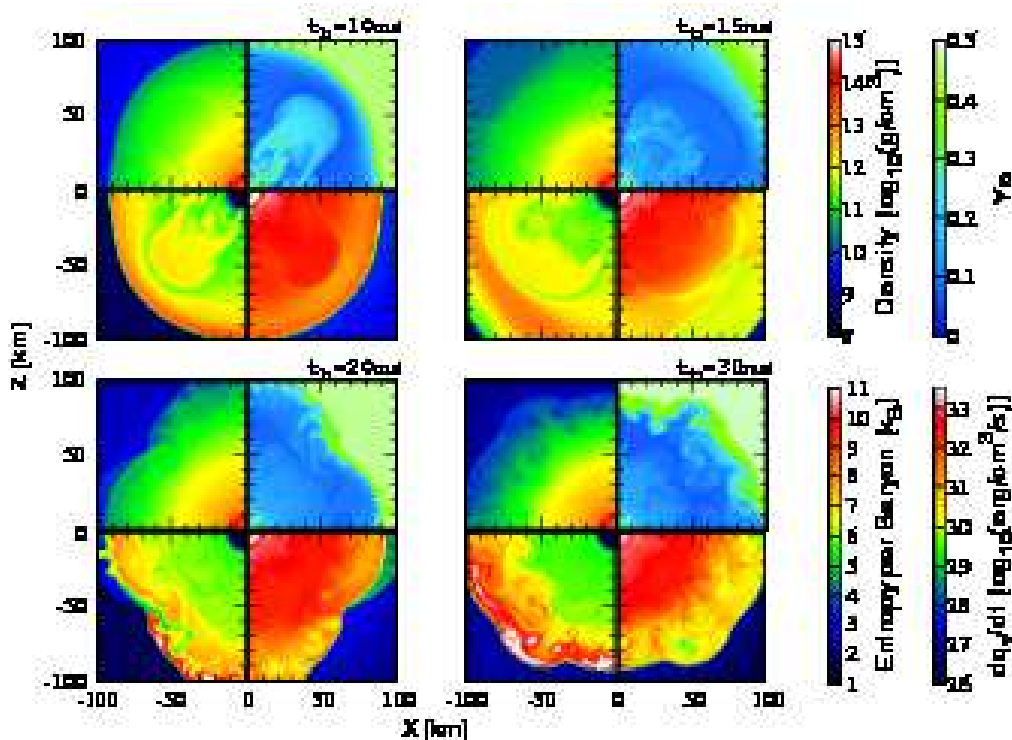


Fig. 5. Snapshots of the contours of the density (top left panels), the electron fraction Y_e (top right panels), the entropy per baryon (bottom left panels), and the local neutrino energy emission rate (bottom right panels) in the x - z plane at selected time slices.

Using this relation, Eq. (6.7) is written as

$$N^2 = \frac{g_{\text{eff}}}{\rho} \left(\frac{d\rho}{dP} \right)_{\text{blob}} \left[\left(\frac{dP}{d\rho} \right)_{\text{blob}} \left(\frac{d\rho}{dr} \right)_{\text{amb}} - \left(\frac{dP}{dr} \right)_{\text{amb}} \right]. \quad (6.9)$$

Because the pressure is a function of the entropy per baryon, the density, and the lepton fraction, $(dP/dr)_{\text{amb}}$ is rewritten to give⁹⁷⁾

$$N^2 = \frac{g_{\text{eff}}}{\rho} \left(\frac{\partial\rho}{\partial P} \right)_{s,Y_l} \left[\left(\frac{\partial P}{\partial s} \right)_{\rho,Y_l} \left(\frac{ds}{dr} \right)_{\text{amb}} + \left(\frac{\partial P}{\partial Y_l} \right)_{\rho,s} \left(\frac{dY_l}{dr} \right)_{\text{amb}} \right]. \quad (6.10)$$

Here, we also assume that the blob elements do not interact the ambient matters both thermally and chemically, i.e. $ds = dY_l = 0$ for the blob. Then, we have

$$\left(\frac{dP}{d\rho} \right)_{\text{blob}} = \left(\frac{\partial P}{\partial\rho} \right)_{s,Y_l}. \quad (6.11)$$

Equation (6.10) shows that when the pressure derivatives of given EOS ($(\partial P/\partial s)_{\rho Y_e}$ and $(\partial P/\partial Y_l)_{\rho s}$) are positive, configurations with negative gradients of entropy and Y_l ($N^2 < 0$) are unstable. (Note that in the above treatment, we have ignored the dissociative effects caused by energy and lepton transports due to neutrinos.) Thus,

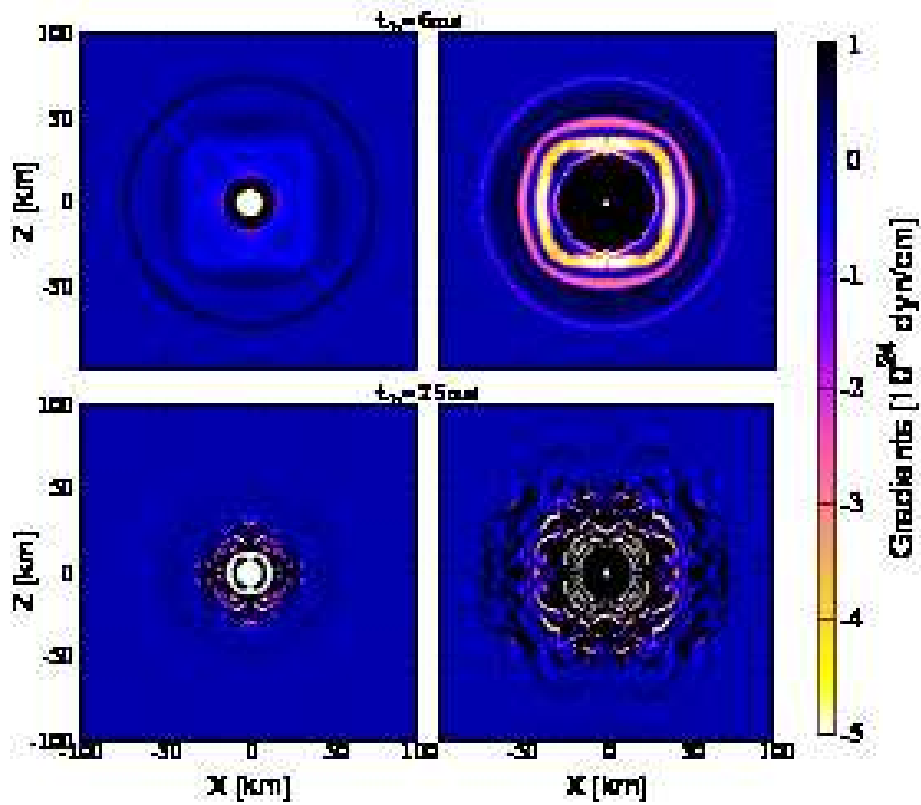


Fig. 6. Snapshots of the contours of gradients associated with the entropy per baryon $(\partial P/\partial s)_{Y_l, \rho}(ds/dr)$ (right panels) and associated with the lepton fraction $(\partial P/\partial Y_l)_{s, \rho}(dY_l/dr)$ (left panels) in the x - z plane at selected time slices.

the negative gradients of the entropy per baryon and the total lepton fraction formed above the neutrino sphere lead to the convective overturn (the proto-neutron star convection). Indeed, convection occurs in our simulation.

Figure 5 shows contours of the density, the electron fraction, the entropy per baryon, and the neutrino energy-emission rate. Convective motions are activated at about 8 ms after the bounce in the region located above the neutrino-sphere where the gradients of the entropy per baryon and Y_l are imprinted (see Fig. 4). At about 10 ms after the bounce, the lepton rich, hot blobs rise to form 'fingers' (see in top left panel in Fig. 5). Note that the neutrino energy emission rate in this finger is relatively higher than that in other region. This is responsible for the small hump seen in the time-evolution of neutrino luminosity (see Fig. 3). Subsequently, the hot fingers expand to form 'mushroom structures', and push the surface of the stalled shock (see top right panel in Fig. 5). At the same time, the lepton poor, colder matters sink down to the proto-neutron star ($r \lesssim 20$ km). The entropy per baryon just behind the shock increases to be $s \gtrsim 10k_B$ and the stalled shock gradually moves outward to reach $r \approx 200$ km. As the hot, lepton rich matters are dug out from the region below the neutrino-sphere, the neutrino luminosity is enhanced (see Fig. 3).

However, the energy released in the convective overturn is not sufficient to keep pushing the shock wave, and eventually, the shock stalls and turns to be a standing accretion shock (bottom two panels of Fig. 5). All these features qualitatively agree with the previous multidimensional Newtonian simulations.^{98),99),100),101),23)} A more detailed comparison with the previous simulations is given in § 6.5.

It will be interesting to investigate which gradient (entropy per baryon or electron fraction) is more responsible for the convection. To see this, we calculate the gradients associated with the entropy per baryon ($\partial P/\partial s)_{Y_l,\rho}(ds/dr)$ (right panels in Fig. 6) and associated with the lepton fraction ($\partial P/\partial Y_l)_{s,\rho}(dY_l/dr)$ (left panels in Fig. 6). This figure clearly shows that negative gradient of the entropy per baryon is more important for the convection activated promptly after the bounce.

6.5. Comparison with the previous studies

To check the validity of the code, the results presented in § 6.2, § 6.3, and § 6.4 are compared with the previous simulations.

6.5.1. Comparison of the results before the convection sets in

We first compare our results with those in the state-of-the-art one-dimensional (1D) simulations in full general relativity,^{15),50),96),16)} in which 1D general relativistic Boltzmann equation is solved for neutrino transfer with relevant weak interaction processes. Because neutrino heating processes ($\nu_e + n \rightarrow p + e^-$ and $\bar{\nu}_e + p \rightarrow n + e^+$) are not included in the present implementation, and on the other hand, multidimensional effects such as convection cannot be followed in the one-dimensional reference simulations, we pay particular attention to comparing results during the collapse and the early phase (~ 10 ms) after the bounce (see results in § 6.2 and § 6.3).

Our radial profiles of the lepton fractions at the bounce (see Fig. 2) approximately agree or at least are consistent with the previous simulations, implying that our code can correctly follow the collapse until the bounce. Also, the radial profiles of the infall velocity, the density, and the entropy per baryon just after the bounce show good agreements with the previous studies. No such good agreement was reported in the previous simulations^{58),61)} where simple leakage schemes based on the single neutrino-trapping density were adopted. Quantitatively, the negative gradients of the entropy per baryon and the lepton fraction are little bit steeper in the present simulation than those in 1D full Boltzmann simulations. The reason may be partly because the *transfers* of lepton-number and energy are not fully solved in the present leakage scheme. Except for this small quantitative difference, the two results agree well.

For validating a scheme for the neutrino cooling, agreement of the neutrino luminosities with those by 1D full Boltzmann simulation should be particularly checked because they depend on both implementations of weak interactions (especially electron capture in the present case) and treatments of neutrino cooling (the detailed leakage scheme). Also, accurate computation of the neutrino luminosities is required for astrophysical applications, because neutrinos carry away the most of energy liberated during the collapse as the main cooling source and can be primary observable.

Our results, in particular the duration and the peak luminosity of the neutrino bursts, agree approximately with those in the previous simulations. Again, no such good agreement was reported in the previous simulation.^{58),61)}

The shock stall-radius is ≈ 80 km. This value is consistent with (although slightly smaller than) that in Liebendörfer et al.⁹⁶⁾ ($R_{\text{stall}} \approx 85$ km) and smaller than that in Sumiyoshi et al.¹⁶⁾ ($R_{\text{stall}} \approx 100$ km). This is likely because in our leakage scheme, neutrino heating is not taken into account.

To summarize, the results in the present simulation agree well with those in the previous 1D Boltzmann simulations qualitatively. Quantitatively, the present results agree approximately with those in the previous 1D Boltzmann simulations. We can obtain approximately correct results with a not computationally expensive scheme without solving the Boltzmann equation. Thus, the present code may be adopted, as a first step, to other multidimensional simulations such as the rotating stellar collapse to a black hole and mergers of compact binaries.

6.5.2. Comparison of the results after the convection sets in

In this section, we compare our results in the convective phase with those in the two-dimensional (2D) Newtonian simulations^{98),99),100),101),23),102),103),72)} in which a wide variety of approximations were adopted for the treatment of neutrinos.

In the present simulation, we have found both the vigorous convective activities (the proto-neutron star convection) and the enhancement of neutrino luminosities due to the convection. These features agree approximately with those in the previous 2D simulations with a fluid-like treatment of neutrinos⁹⁹⁾ and with radial ray-by-ray, gray flux-limited diffusion approximation of neutrino transfers.^{98),100),101)} In a spherically symmetric, gray flux-limited diffusion scheme,¹⁰²⁾ by contrast, only mildly active convection was found and no enhancement in the neutrino luminosities was observed.

Note that the transport of energy and lepton number by neutrinos can flatten the negative gradients of entropy and lepton fraction, and as a result, the convection will be suppressed. In purely hydrodynamic simulations without neutrino processes^{23),102)} (using a postbounce core obtained in 1D simulations with neutrinos), the proto-neutron star convection is strongly activated. In the radial ray-by-ray simulations,^{98),100),101)} the transfer of neutrinos in the angular direction is not taken into account and the stabilizing effect is underestimated, resulting in the proto-neutron star convection with the enhancement of neutrino luminosities. In the spherically symmetric simulation,¹⁰²⁾ the transfer of neutrino in the angular direction is assumed to occur fast enough to make the neutrino distribution function spherically symmetric, and consequently, the stabilizing effect is overestimated.

Recently, Buras et al.⁷²⁾ performed simulations with a modified ray-by-ray, multi-group scheme in which some part of the lateral components are included, and found that the proto-neutron star convection indeed sets in but has minor effects on the enhancement of the neutrino luminosities. Dessart et al.¹⁰³⁾ performed simulations employing a 2D multi-group flux-limited diffusion scheme and found similar results as in Buras et al. Thus, although the proto-neutron star convection indeed occurs, its influence on enhancing the neutrino luminosities may be minor. The

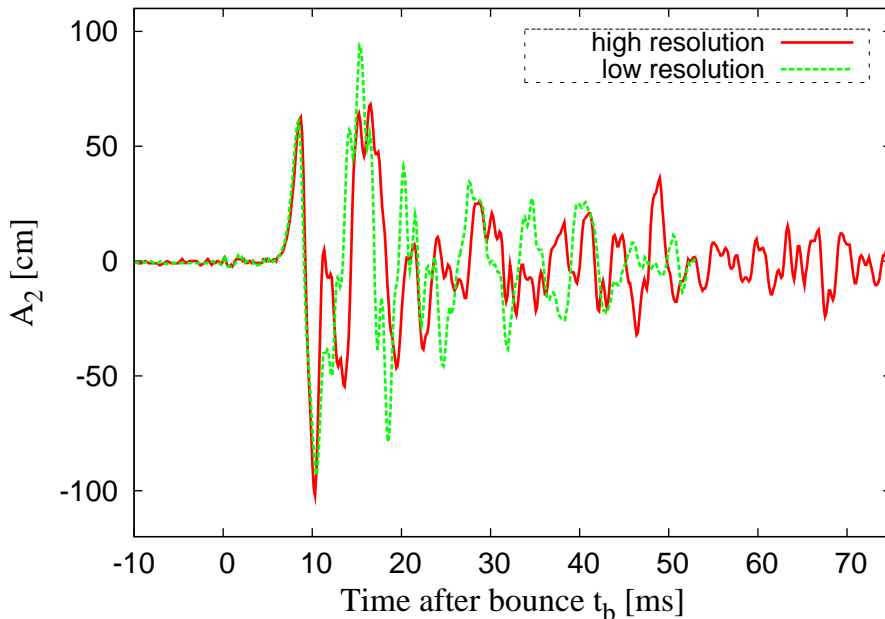


Fig. 7. Gravitational wave quadrupole amplitude A_2 due to the prompt convection as a function of post bounce time t_b . The results for the finer grid resolution (solid curve) and for the coarser grid resolution (the dotted curves) are shown together.

strong convective activities and the enhancement of neutrino luminosities found in the present simulation should be considered as the maximum ones.

Note that it is in intermediate regions ($\tau_\nu \sim 1$) that the stabilizing effect due to the neutrino transfer works efficiently: At higher density region with $\tau_\nu \gg 1$, neutrinos cannot efficiently transport the energy and the lepton number due to the large opacities; At lower density region with $\tau_\nu \ll 1$, on the other hand, neutrinos carry away the energy and the lepton number without interacting with the matter. Therefore a careful and detailed treatment of the neutrino transfer is required to clarify the degree of the stabilizing effect and the convection, although such a computationally expensive simulation is beyond the scope of this paper.

The present result that the proto-neutron star convection occurs qualitatively agrees with the recent simulations with detailed neutrino transfer.^{103),72)} If simulations are performed keeping in mind that the stabilizing effect due to the neutrino transfer is not taken into account in the present scheme, the present code will be acceptable to explore the the rotating stellar collapse to a black hole and mergers of compact binaries.

6.6. Gravitational radiation

Associated with the convective motions, gravitational waves are emitted. The gravitational waveforms are computed using a quadrupole formula.¹⁰⁴⁾ In quadrupole formulae, only the +-mode of gravitational waves with $l = 2$ and $m = 0$ is nonzero

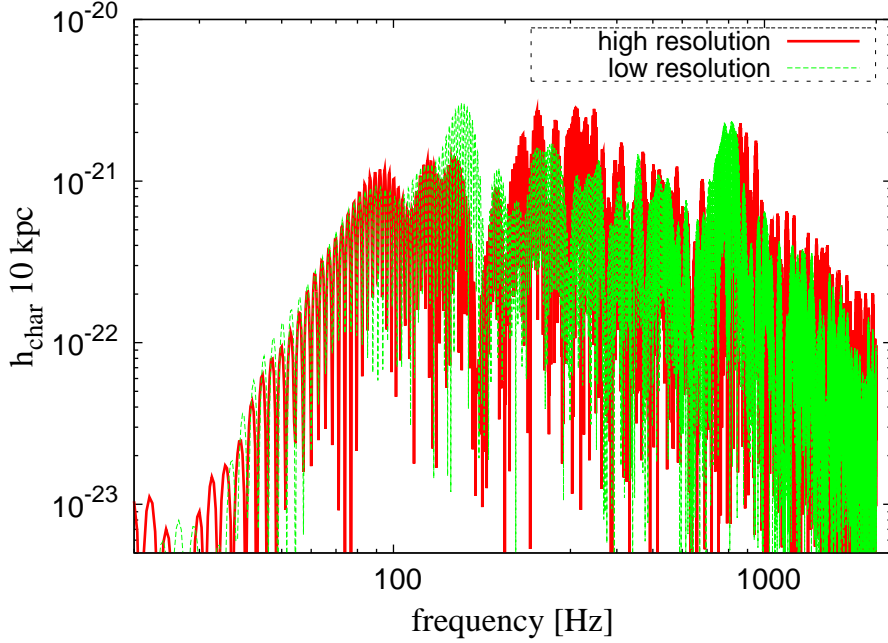


Fig. 8. The frequency spectra of the characteristic gravitational-wave strain due to the prompt convection. The results for the finer grid resolution (solid curve) and for the coarser grid resolution (the dotted curves) are shown together.

in axisymmetric spacetime and is written as

$$h_+^{\text{quad}} = \frac{\ddot{I}_{zz}(t_{\text{ret}}) - \ddot{I}_{xx}(t_{\text{ret}})}{r} \sin^2 \theta \equiv \frac{A_2(t)}{r} \sin^2 \theta, \quad (6.12)$$

where I_{ij} denotes a quadrupole moment, \ddot{I}_{ij} its second time derivative, and t_{ret} a retarded time. In fully general relativistic and dynamical spacetime, there is no unique definition for the quadrupole moment and nor is for \dot{I}_{ij} . Following Shibata and Sekiguchi,¹⁰⁴⁾ we choose the simplest definition of the form

$$I_{ij} = \int \rho_* x^i x^j d^3x. \quad (6.13)$$

Then, using the continuity equation, the first time derivative can be written as

$$\dot{I}_{ij} = \int \rho_* (v^i x^j + x^i v^j) d^3x, \quad (6.14)$$

and \ddot{I}_{ij} is computed by the finite differencing of the numerical result for \dot{I}_{ij} . In the following, we present A_2 , which provides the amplitude of a given mode measured by an observer located in the most optimistic direction (in the equatorial plane). We also calculate the characteristic gravitational-wave strain,¹⁰⁵⁾

$$h_{\text{char}}(f) \equiv \sqrt{\frac{2}{\pi^2} \frac{G}{c^3} \frac{1}{D^2} \frac{dE}{df}}, \quad (6.15)$$

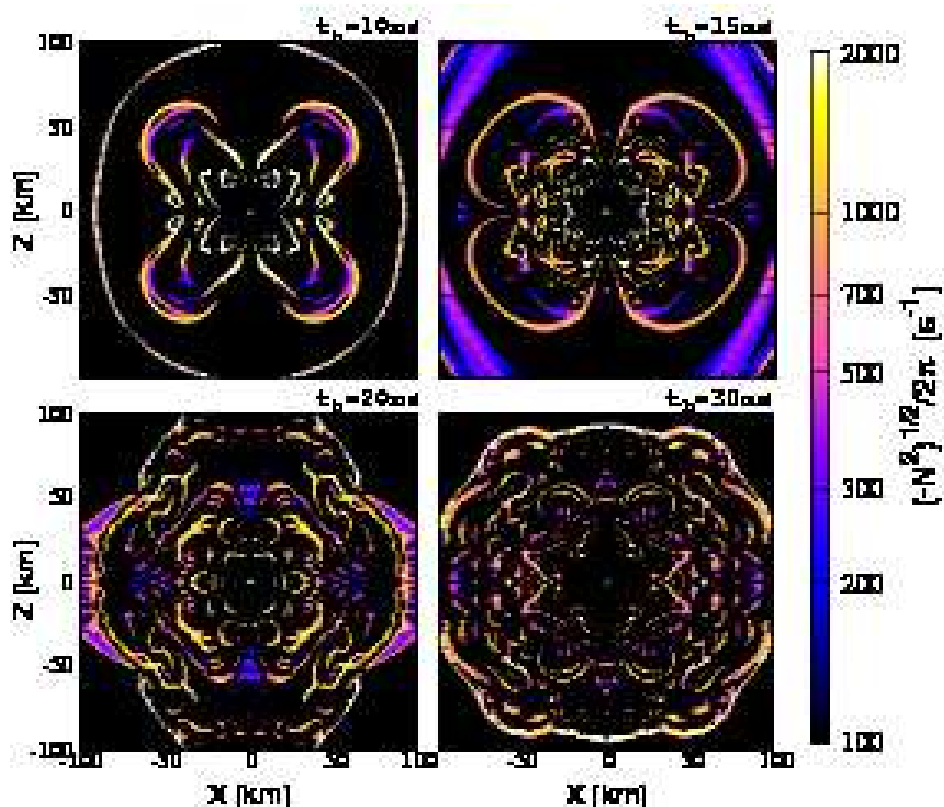


Fig. 9. Snapshots of the contours of $\sqrt{-N^2}/2\pi$, in the x - z plane at selected time slices.

where

$$\frac{dE}{df} = \frac{8\pi^2 c^3}{15 G} f^2 \left| \tilde{A}_2(f) \right|^2 \quad (6.16)$$

is the energy power spectra of the gravitational radiation and

$$\tilde{A}_2(f) = \int A_2(t) e^{2\pi i f t} dt. \quad (6.17)$$

Figure 7 shows $A_2(t)$. Because the system is initially spherically symmetric, no gravitational radiation is emitted before the onset of the convection. When the proto-neutron star convection sets in at ≈ 10 ms after the bounce, gravitational waves start to be emitted. The peak amplitudes are $A_2 \sim 100$ cm. After the peak is reached, gravitational waves generated by the smaller-scale convective motions are emitted with $A_2 \approx 50$ cm.

Figure 8 shows the spectra of h_{char} due to the convective motions. In contrast to the spectra due to the core bounce (e.g. Refs. 20) and 30)), there is no dominant peak frequency in the power spectra. Instead, several maxima for the frequency range 100–1000 Hz are present. Note that for gravitational waves due to the core bounce, the characteristic peak frequency is associated with the bounce timescale of the core. The effective amplitude of gravitational waves observed in the most

optimistic direction is $h_{\text{char}} \approx 6\text{--}8 \times 10^{-21}$ for an event at a distance of 10 kpc, which is as large as that emitted at the bounce of rotating core collapse.²⁰⁾

To check that gravitational waves are indeed originated by the convective motions, we calculate the frequency $\sqrt{-N^2}/2\pi$ (see Eq. (6.7)) as shown in Fig. 9. This frequency is in good agreement with the gravitational-wave frequency, implying that gravitational waves are indeed due to the convective activities.

Müller and Janka²³⁾ investigated gravitational waves due to the convective motion inside the proto-neutron star. It is interesting to compare our results with theirs. They adopted a post-bounce model of Hillebrandt.¹⁰⁶⁾ They put an inner boundary at radius $r_{\text{in}} = 15$ km and assumed the hydrostatic equilibrium there. They do not include neutrino transfer while a sophisticated EOS is adopted. They found qualitatively similar results to ours. According to their results, the maximum amplitude of the quadrupole mode is $A_2 \approx 100$ cm, which agrees well with our results. The spectrum of the gravitational-wave strain has several maxima for $f = 50\text{--}500$ Hz with the maximum value of $h_{\text{char}} \approx 3 \times 10^{-21}$. The peaks in h_{char} are distributed for higher frequency side in our results probably due to the general relativistic effects. We note that a similar general relativistic effect is observed for gravitational waves at the bounce phase.²⁰⁾ These facts show that for deriving quantitatively correct spectra of gravitational waves, fully general relativistic simulations are necessary.

6.7. Numerical accuracy

In Figs. 1–3 we show the results both in the higher resolution (solid curves) and in the lower resolution (dashed curves). The radial profiles of the two resolutions are almost identical, showing that convergent results are obtained in the present simulation (see Fig. 4). In the time evolution of neutrino luminosities (see Fig. 3), the two results are almost identical before the convective activities set in. In the later phase, on the other hand, the two results show slight disagreement. Because the convection and the turbulence can occur in an infinitesimal scale length, the smaller-scale convection and turbulence are captured in the finer grid resolution. However, the influence of the grid resolution on the neutrino luminosities is minor because the convection and turbulence are strongly activated in the region above the neutrino sphere (see the contours of the electron fraction and the entropy in Fig. 5). On the other hand, most of the neutrinos are emitted from the region inside the neutrino sphere (see the contour of the local neutrino energy emission rate in Fig. 5).

The effect of the grid resolution can be seen in gravitational waves. In Figs. 7 and 8 we show the quadrupole mode $A_2(t)$ and the characteristic strain $h_{\text{char}}(f)$ both in the higher resolution (solid curves) and in the lower resolution (dashed curves). After the formation of the lepton-rich, hot finger at ≈ 10 ms after the bounce (see § 6.4), convective activities set in. Then, disagreement of $A_2(t)$ between the finer and the coarser grid resolutions becomes noticeable (see Fig. 7). The characteristic peaks of $h_{\text{char}}(f)$ in higher frequencies ($f \sim 200\text{--}500$ Hz) are more prominent (see Fig. 8). It is likely to be because the smaller-scale turbulent motions are captured in the finer grid resolution.

To check the accuracy of our numerical results, the violation of the Hamiltonian

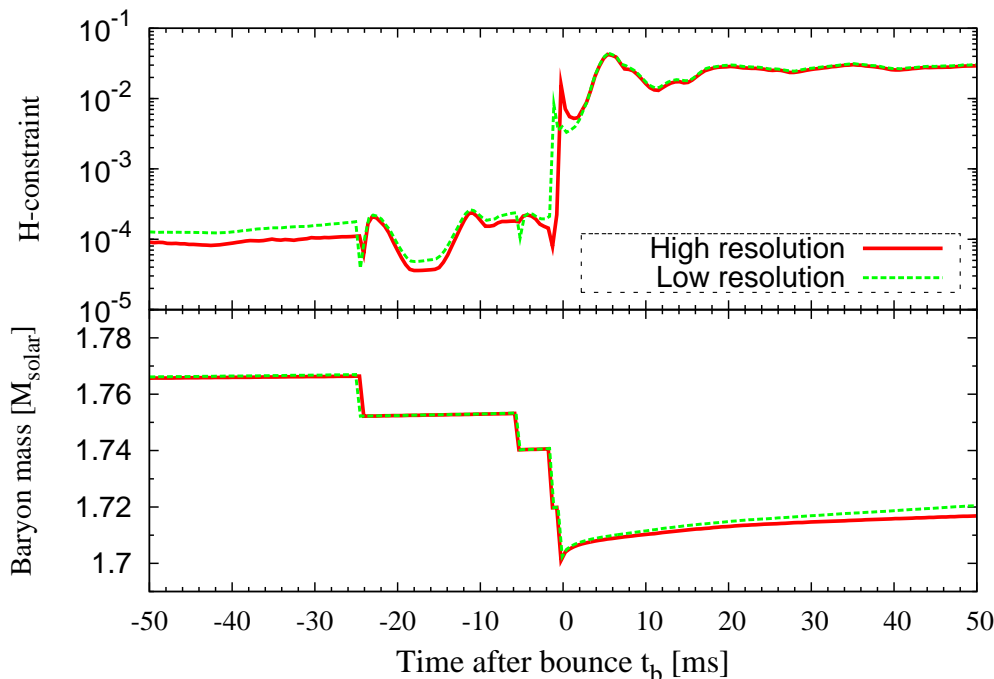


Fig. 10. Evolution of the averaged violation of the Hamiltonian constraint (upper panel) and baryon mass conservation (lower panel).

constraint are calculated, which is written as

$$H = -8\psi^{-5} \left[\tilde{\Delta}\psi - \frac{\psi}{8}\tilde{R} + 2\pi\rho_h\psi^5 + \frac{\psi^5}{8}\tilde{A}_{ij}\tilde{A}^{ij} - \frac{\psi^5}{12}K^2 \right], \quad (6.18)$$

where $\psi \equiv e^\phi$, and $\tilde{\Delta}$ denotes the Laplacian with respect to $\tilde{\gamma}_{ij}$. In this paper, the averaged violation is defined according to⁸⁹⁾

$$\text{ERROR} = \frac{1}{M_*} \int \rho_* |V| d^3x, \quad (6.19)$$

where M_* is the rest-mass density of the core (see Eq. 6.1)

$$V = \frac{\tilde{\Delta}\psi - \frac{\psi}{8}\tilde{R} + 2\pi E\psi^5 + \frac{\psi^5}{8}\tilde{A}_{ij}\tilde{A}^{ij} - \frac{\psi^5}{12}K^2}{|\tilde{\Delta}\psi| + \left| \frac{\psi}{8}\tilde{R} \right| + 2\pi\rho_h\psi^5 + \frac{\psi^5}{8}\tilde{A}_{ij}\tilde{A}^{ij} + \frac{\psi^5}{12}K^2}. \quad (6.20)$$

Namely, we use ρ_* as a weight factor for the average. This weight factor is introduced to monitor whether the main bodies of the system (proto-neutron stars and inner cores), in which we are interested, are accurately computed or not.

We display the time evolution of the Hamiltonian-constraint violation and the conservation of the baryon mass of the system in Fig. 10. Several discontinuous

changes in the Hamiltonian-constraint violation and the conservation of the baryon mass originate from the regridding procedures in which some matters of the outer region are discarded.

Before the bounce, the baryon mass is well conserved and the Hamiltonian-constraint violation is very small as $\sim 10^{-4}$. After the bounce, the violation of the baryon-mass-conservation and the Hamiltonian constraint is enhanced due to the existence of shock waves where the hydrodynamic scheme becomes essentially a first-order scheme. The convergence of the baryon-mass-conservation and the Hamiltonian-constraint violation also becomes worse in the convective phase. However, the degree of violation of the Hamiltonian constraint and the baryon-mass-conservation is small and we may believe that the numerical results obtained in the paper are reliable.

§7. Summary and Discussion

7.1. Summary

In this paper, we present a fully general relativistic hydrodynamic code in which a finite-temperature EOS and neutrino cooling are implemented for the first time. Because the characteristic timescale of weak interaction processes $t_{\text{wp}} \sim |Y_e/\dot{Y}_e|$ (WP timescale) is much shorter than the dynamical timescale t_{dyn} in hot dense matters, stiff source terms appear in the equations. In general, an implicit scheme may be required to solve them.⁶⁵⁾ However, it is not clear whether implicit schemes do work or not in the relativistic framework. The Lorentz factor is coupled with the rest-mass density and the energy density. The specific enthalpy is also coupled with the momentum. Due to these couplings, it is not straightforward to recover the primitive variables and the Lorentz factor from conserved quantities. Taking account of these facts, we proposed an explicit method to solve all the equations noting that the characteristic timescale of neutrino leakage from the system t_{leak} is much longer than t_{wp} and is comparable to t_{dyn} .

By decomposing the energy-momentum tensor of neutrinos into the trapped-neutrino and the streaming-neutrino parts, the hydrodynamic equations can be rewritten so that the source terms are characterized by the leakage timescale t_{leak} (see Eqs. (3.8) and (3.5)). The lepton-number conservation equations, on the other hand, include the source terms characterized by the WP timescale. Taking account of these facts, *limiters* for the stiff source terms are introduced to solve the lepton-number conservation equations explicitly (see § 3.2). In the numerical relativistic hydrodynamics, it is required to calculate the primitive variables and the Lorentz factor from the conserved quantities. In this paper, we develop a robust and stable procedure for it (§ 5.3).

To check the validity of the numerical code, we performed a simulation of spherical stellar core collapse. As initial conditions, we adopted the $15M_{\odot}$ spherical model with the solar metallicity computed by Woosley et al.⁹⁴⁾ After the shock formation and propagation, the shock wave suffers from the severe reduction of its energy due to neutrino burst emission when the shock wave passes the neutrino-sphere. Even-

tually, the shock wave stalls soon after it passes through the neutrino sphere. The neutrino burst makes negative gradients of the entropy and Y_l above the neutrino sphere. Because such configuration is convectively unstable, vigorous convective motions are induced. All these properties agree qualitatively with those by the recent 2D Newtonian simulations.^{103), 72)}

We also compared our results with those in the previous simulations. Before the convection sets in, we compare our result with those in the state-of-the-art 1D Boltzmann simulations in full general relativity.^{15), 50), 36), 16)} As shown in this paper, the radial structure of the core and the neutrino luminosities agree qualitatively well with those in their simulations. Quantitatively, they also agree approximately with the previous results.

After the convection sets in, we compare our result with those in 2D Newtonian simulations.^{98), 99), 100), 101), 23), 102), 103), 72)} Our result that the proto-neutron star convection occurs agree qualitatively with that in the previous simulations.^{98), 99), 100), 101), 23), 103), 72)} However, quantitative properties show disagreement because the transfer of neutrinos are not fully solved in the present scheme. Note that the transport of energy and lepton-number by neutrinos can flatten the negative gradients of entropy and lepton fraction, stabilizing the convection. Therefore the convective activities obtained in the present simulation should be considered as the maximum ones.

If we keep in mind the above facts and note the good agreements of the radial structure and neutrino luminosities, the present implementation will be applied to simulations of rotating core collapse to a black hole and mergers of binary neutron stars as a first step towards more sophisticated models. A detailed treatment of the neutrino transfer is required to determine the degree of stabilizing effect, but this is far beyond the scope of this paper.

Gravitational waves emitted by the convective motions are also calculated. The gravitational-wave amplitude is $\approx 3 \times 10^{-21}$ for an event of the distance 10 kpc. Reflecting the contributions of multi-scale eddies with characteristic overturn timescale 1–10 ms, the energy power spectrum shows several maxima distributed in $f \approx 100$ –1000 Hz. We compare our results with those in Müller and Janka²³⁾ in which a similar calculation (but in Newtonian gravity) is performed. The maximum amplitude of gravitational waves in our results agrees well with that in Müller and Janka. The several maxima in the energy power spectrum are distributed at higher-frequency side in our results due to the general relativistic effects, showing that fully general relativistic simulations are necessary for the accurate calculation of gravitational-wave spectra.

7.2. Discussions

Because the present implementation of the microphysics is simple and explicit, it has advantage that the individual microphysical processes can be easily improved and sophisticated. For example, the neutrino emission via the electron capture can be easily sophisticated as follows. To precisely calculate the electron capture rate, the complete information of the parent and daughter nuclei is required. In EOSs currently available, however, a representative single-nucleus average for the true ensemble of heavy nuclei is adopted. The representative is usually the most

abundant nucleus. The problem in evaluating the capture rate is that the nuclei which cause the largest changes in Y_e are neither the most abundant nuclei nor the nuclei with the largest rates, but the combination of the two. In fact, the most abundant nuclei tend to have small rates because they are more stable than others, and the fraction of the most reactive nuclei tend to be small.^{107),9)} Assuming that the nuclear statistical equilibrium (NSE) is achieved, the electron capture rates under the NSE ensemble of heavy nuclei may be calculated for a given set of (ρ, Y_e, T) . Such a numerical rate table can be easily employed in the present implementation.

Also, the neutrino cross sections can be improved. As summarized in Ref. 108), there are a lot of corrections to the neutrino opacities. Note that small changes in the opacities may result in much larger changes in the neutrino luminosities, because the neutrino energy emission rates depend strongly on the temperature, and the temperature at the last scattering surface ($\tau_\nu \sim \sigma T^2 \sim 1$) changes as $T \sim \sigma^{-1/2}$. Although the correction terms are in general very complicated, it is straightforward to include the corrections into our code. Note that the corrections become more important for higher neutrino energies. Therefore, the correction terms might play a crucial role in the collapse of population III stellar core and the formation of a black hole, in which very high temperatures ($T > 100$ MeV) will be achieved. A study to explore the importance of these corrections in the case of black hole formation is ongoing.

As briefly described in the introduction, one of the main drawbacks in the present implementation of the neutrino cooling is that the *transfer* of neutrinos are not solved. Although *fully* solving the transfer equations of neutrinos is far beyond the scope of this paper, there are a lot of rooms for improvements in the treatment of the neutrino cooling. For example, the relativistic moment formalism,^{109),110)} in particular the so-called M1 closure formalism, may be adopted. For this purpose, a more sophisticated treatment of the closure relation for $P_{\alpha\beta}$ is required. We plan to implement a relativistic M1 closure formalism for the neutrino transfer in the near future.

To conclude, the present implementation of microphysics in fully general relativistic, multidimensional code works well and has a wide variety of applications. We are now in the standpoint where simulations of stellar core collapse to a black hole and merger of compact stellar binaries can be performed including microphysical processes. Fruitful scientific results will be reported in the near future.

acknowledgments

The author thanks M. Shibata for valuable discussions and careful reading of the manuscript, and L. Rezzolla, and K. Sumiyoshi for valuable discussions. He also thanks T. Shiromizu and T. Fukushige for their grateful aids. He thanks S. E. Woosley, A. Heger and T. A. Weaver for providing the presupernova core used in the present simulation as an initial condition. Numerical computations were performed on the NEC SX-9 at the data analysis center of NAOJ and on the NEC SX-8 at YITP in Kyoto University. This work is partly supported by the Grant-in-Aid of the Japanese Ministry of Education, Science, Culture, and Sport (21018008,21105511).

Appendix A

— Electron and positron captures —

In this section, we briefly summarize our treatments of electron and positron captures which are based on Ref. 66) and give the explicit forms of $\gamma_{\nu e}^{\text{ec}}$, $\gamma_{\bar{\nu} e}^{\text{pc}}$, $Q_{\nu e}^{\text{ec}}$, and $Q_{\bar{\nu} e}^{\text{pc}}$ appeared in Eqs. (3·27), (3·28), and (3·30), for the purpose of convenience.

A.1. The electron and positron capture rates $\gamma_{\nu e}^{\text{ec}}$ and $\gamma_{\bar{\nu} e}^{\text{pc}}$

The 'net' electron fraction is written as $Y_e = Y_- - Y_+$ where Y_- (Y_+) denotes the number of electrons (positrons) per baryon including pair electrons. Then the electron-neutrino number emission rate by the electron capture and the electron-anti-neutrino number emission rate by the positron capture are given by

$$\gamma_{\nu e}^{\text{local}} = -\dot{Y}_- = -(\dot{Y}_-^f + \dot{Y}_-^h), \quad (\text{A}\cdot 1)$$

$$\gamma_{\bar{\nu} e}^{\text{local}} = -\dot{Y}_+ = -(\dot{Y}_+^f + \dot{Y}_+^h), \quad (\text{A}\cdot 2)$$

where the electron and positron capture rates are decomposed into two parts, capture on by free nucleons (with superscript f) and on heavy nuclei (with superscript h). In the following, we present the explicit forms of \dot{Y}_-^f , \dot{Y}_+^f , \dot{Y}_-^h , and \dot{Y}_+^h .

A.2. Capture on free nucleons \dot{Y}^f

The electron capture rate (including the contribution of the inverse reaction of the neutrino capture) on free nucleons (\dot{Y}_-^f) is given by

$$\dot{Y}_-^f = X_n \lambda^{\nu e c, f} - X_p \lambda^{\text{ec}, f}, \quad (\text{A}\cdot 3)$$

where $\lambda^{\text{ec}, f}$ is the specific electron capture rate on free protons, $\lambda^{\nu e c, f}$ is the specific electron-neutrino capture rate on free neutrons, and X_p and X_n are the mass fraction of free proton and neutron, respectively. Based on a balance argument,⁶⁶⁾ one can show that $\lambda^{\nu e c, f}$ is related to $\lambda^{\text{ec}, f}$ by

$$\lambda^{\nu e c, f} = \exp\left(\eta_{\nu e} - \eta_e - \frac{\delta m}{k_B T}\right) \lambda^{\text{ec}, f}, \quad (\text{A}\cdot 4)$$

where $\eta_{\nu e}$ and η_e are the chemical potentials of electron neutrinos and electrons in units of $k_B T$ and $\delta m = (m_n - m_p)c^2$. Furthermore, we use the following relation for non-degenerate free nucleons,

$$X_n \approx X_p \exp\left(\eta_n - \eta_p + \frac{\delta m}{k_B T}\right), \quad (\text{A}\cdot 5)$$

where η_n and η_p are the chemical potentials of free neutrons and free protons in units of $k_B T$. Then we obtain

$$\dot{Y}_-^f = [\exp(\eta_{\nu e} - \eta_e + \eta_n - \eta_p) - 1] X_p \lambda^{\text{ec}, f}. \quad (\text{A}\cdot 6)$$

The positron capture rate (including the contribution of the inverse reaction) on free nucleons is similarly given by

$$\dot{Y}_+^f = X_p \lambda^{\bar{\nu} e c, f} - X_n \lambda^{\text{pc}, f} = [\exp(\eta_{\bar{\nu} e} + \eta_e + \eta_p - \eta_n) - 1] X_n \lambda^{\text{pc}, f}, \quad (\text{A}\cdot 7)$$

where $\eta_{\bar{\nu}e}$ is the chemical potential of electron-anti-neutrinos in units of $k_B T$, λ^{pc} is the specific positron capture rate on free neutrons, and $\lambda^{\bar{\nu}e,c,f}$ is the specific electron-anti-neutrino capture rate on free protons.

A.3. Capture on heavy nuclei \dot{Y}^h

The electron capture rate (including the contribution of the inverse reaction of the neutrino capture) on a heavy nucleus of mass number A (\dot{Y}_-^h) is given by⁶⁶⁾

$$\dot{Y}_-^h = \frac{X_D}{A} \lambda^{\nu_e c, h} - \frac{X_P}{A} \lambda^{\text{ec}, h}, \quad (\text{A}\cdot 8)$$

where $\lambda^{\text{ec}, h}$ is the specific electron capture rate on the parent nucleus (mass fraction X_P), $\lambda^{\nu_e c, h}$ is the specific electron neutrino capture rate on the daughter nucleus (mass fraction X_D), and A is the atomic mass of the parent and daughter nuclei. In the present simulations, we set $X_D = X_P = X_A$. Then, under the assumption of nuclear statistical equilibrium, one may approximate the capture rate on heavy nuclei as,⁶⁶⁾

$$\dot{Y}_-^h \approx [\exp(\eta_{\nu e} - \eta_e + \eta_n - \eta_p) - 1] \frac{X_A}{A} \lambda^{\text{ec}, h}. \quad (\text{A}\cdot 9)$$

Similarly, the positron capture rate (including the contribution of the inverse reaction) on heavy nuclei (\dot{Y}_+^h) is given by

$$\dot{Y}_+^h = \frac{X_D}{A} \lambda^{\bar{\nu}e c, h} - \frac{X_P}{A} \lambda^{\text{pc}, h} \approx [\exp(\eta_{\bar{\nu}e} + \eta_e + \eta_p - \eta_n) - 1] \frac{X_A}{A} \lambda^{\text{pc}, h}. \quad (\text{A}\cdot 10)$$

A.4. The specific capture rate λ

The specific electron and positron capture rates on free nucleons and on heavy nuclei and are written in the same form as⁶⁶⁾

$$\lambda^{\text{ec}, f} = \frac{\ln 2}{\langle ft \rangle_{\text{eff}}^{\text{ec}, f}} I^{\text{ec}, f}, \quad \lambda^{\text{pc}, f} = \frac{\ln 2}{\langle ft \rangle_{\text{eff}}^{\text{pc}, f}} I^{\text{pc}, f}, \quad (\text{A}\cdot 11)$$

$$\lambda^{\text{ec}, h} = \frac{\ln 2}{\langle ft \rangle_{\text{eff}}^{\text{ec}, h}} I^{\text{ec}, h}, \quad \lambda^{\text{pc}, h} = \frac{\ln 2}{\langle ft \rangle_{\text{eff}}^{\text{pc}, h}} I^{\text{pc}, h}, \quad (\text{A}\cdot 12)$$

where $I^{\text{ec}, f}$ and $I^{\text{pc}, f}$ are the phase space factors for the electron and positron captures on free electrons, and $I^{\text{ec}, h}$ and $I^{\text{pc}, h}$ are those on heavy nuclei. $\langle ft \rangle_{\text{eff}}$'s are the effective ft -values introduced by Fuller et al.,⁶⁶⁾ which is essentially the same as the square of the nuclear transition matrix.

The phase space factors are given by

$$I^{\text{ec}, f} = \left(\frac{k_B T}{m_e c^2} \right)^5 \int_{\eta_0}^{\infty} \eta^2 (\eta + \zeta^{\text{ec}, f})^2 \frac{1}{1 + e^{\eta - \eta_e}} \left[1 - \frac{1}{1 + e^{\eta - \eta_{\nu e} + \zeta^{\text{ec}, f}}} \right] d\eta, \quad (\text{A}\cdot 13)$$

$$I^{\text{pc}, f} = \left(\frac{k_B T}{m_e c^2} \right)^5 \int_{\eta_0}^{\infty} \eta^2 (\eta + \zeta^{\text{pc}, f})^2 \frac{1}{1 + e^{\eta + \eta_e}} \left[1 - \frac{1}{1 + e^{\eta - \eta_{\bar{\nu}e} + \zeta^{\text{pc}, f}}} \right] d\eta, \quad (\text{A}\cdot 14)$$

$$I^{\text{ec}, h} = \left(\frac{k_B T}{m_e c^2} \right)^5 \int_{\eta_0}^{\infty} \eta^2 (\eta + \zeta^{\text{ec}, h})^2 \frac{1}{1 + e^{\eta - \eta_e}} \left[1 - \frac{1}{1 + e^{\eta - \eta_{\nu e} + \zeta^{\text{ec}, h}}} \right] d\eta, \quad (\text{A}\cdot 15)$$

$$I^{\text{pc},h} = \left(\frac{k_B T}{m_e c^2} \right)^5 \int_{\eta_0}^{\infty} \eta^2 (\eta + \zeta^{\text{pc},h})^2 \frac{1}{1 + e^{\eta + \eta_e}} \left[1 - \frac{1}{1 + e^{\eta - \eta_{\bar{\nu}e} + \zeta^{\text{pc},h}}} \right] d\eta, \quad (\text{A}\cdot 16)$$

where $\zeta^{\text{ec},f}$, $\zeta^{\text{pc},f}$, $\zeta^{\text{ec},h}$, and $\zeta^{\text{pc},h}$ are the nuclear mass-energy differences for electron capture and positron capture in units of $k_B T$. The nuclear mass-energy differences for capture on free nuclei are given by

$$\zeta^{\text{ec},f} = -\zeta_n^{\text{pc},f} \approx \eta_p - \eta_n. \quad (\text{A}\cdot 17)$$

We follow Fuller et al.⁶⁶⁾ for the nuclear mass-energy differences for capture on heavy nuclei: In the case of $N < 40$ or $Z > 20$ (referred to as 'unblocked' case), we set

$$\zeta^{\text{ec},h} = -\zeta^{\text{pc},h} \approx \eta_p - \eta_n. \quad (\text{A}\cdot 18)$$

In the case of $N \geq 40$ or $Z \leq 20$ (referred to as 'blocked' case), on the other hand, we set

$$\zeta^{\text{ec},h} \approx \eta_p - \eta_n - \frac{5(\text{MeV})}{k_B T}, \quad (\text{A}\cdot 19)$$

$$\zeta^{\text{pc},h} \approx -\eta_p + \eta_n + \frac{5(\text{MeV})}{k_B T}. \quad (\text{A}\cdot 20)$$

Then, the threshold value of the electron and positron captures is given by $\eta_0 = m_e c^2 / (k_B T)$ for $\zeta > -m_e c^2 / (k_B T)$ and $\eta_0 = |\zeta|$ for $\zeta < -m_e c^2 / (k_B T)$ where we have dropped the superscripts 'ec', 'pc', 'f', and 'h' in ζ for simplicity.

The effective ft -value of electron or positron capture on free nuclei is given by (e.g. Ref. 66)

$$\log_{10} \langle ft \rangle_{\text{eff}}^{\text{ec},f} = \log_{10} \langle ft \rangle_{\text{eff}}^{\text{pc},f} \approx 3.035. \quad (\text{A}\cdot 21)$$

We follow Fuller et al.⁶⁶⁾ for the effective ft -value of capture on heavy nuclei, who proposed to use

$$\log_{10} \langle ft \rangle_{\text{eff}}^{\text{ec},h} \approx \begin{cases} 3.2 & \text{unblocked} & \eta_e < |\zeta^{\text{ec},h}| \\ 2.6 & \text{unblocked} & \eta_e > |\zeta^{\text{ec},h}| \\ 2.6 + \frac{25.9}{T_9} & \text{blocked} \end{cases}, \quad (\text{A}\cdot 22)$$

$$\log_{10} \langle ft \rangle_{\text{eff}}^{\text{pc},h} \approx \begin{cases} 3.2 & \text{unblocked} & \eta_e < |\zeta^{\text{pc},h}| \\ 2.6 & \text{unblocked} & \eta_e > |\zeta^{\text{pc},h}| \\ 2.6 + \frac{25.9}{T_9} & \text{blocked} \end{cases}, \quad (\text{A}\cdot 23)$$

where $T_9 = T / (10^9 K)$. In this expression, the thermal unblocking effect⁶⁷⁾ is readily taken into account. In the thermal unblocking, it costs ≈ 5.13 MeV to pull a neutron out of a filled orbital $1f_{5/2}$ and place it in the gd -shell.⁶⁶⁾

A.5. Energy emission rates $Q_{\nu e}^{\text{ec}}$ and $Q_{\bar{\nu}e}^{\text{pc}}$

The neutrino energy emission rates associated with electron and positron captures in units of $m_e c^2 \text{ s}^{-1}$ are given by⁶⁶⁾

$$\pi^{\text{ec}} = \ln 2 \frac{J^{\text{ec}}}{\langle ft \rangle_{\text{eff}}^{\text{ec}}}, \quad \pi^{\text{pc}} = \ln 2 \frac{J^{\text{pc}}}{\langle ft \rangle_{\text{eff}}^{\text{pc}}}, \quad (\text{A}\cdot 24)$$

where the phase space factors are given by

$$J^{\text{ec}} = \left(\frac{k_B T}{m_e c^2} \right)^6 \int_{\eta_0}^{\infty} \eta^2 (\eta + \zeta^{\text{ec}})^3 \frac{1}{1 + e^{\eta - \eta_e}} \left[1 - \frac{1}{1 - e^{\eta - \eta_{\nu_e} + \zeta^{\text{ec}}}} \right] d\eta, \quad (\text{A}\cdot 25)$$

$$J^{\text{pc}} = \left(\frac{k_B T}{m_e c^2} \right)^6 \int_{\eta_0}^{\infty} \eta^2 (\eta + \zeta^{\text{pc}})^3 \frac{1}{1 + e^{\eta + \eta_e}} \left[1 - \frac{1}{1 - e^{\eta - \eta_{\bar{\nu}_e} + \zeta^{\text{pc}}}} \right] d\eta. \quad (\text{A}\cdot 26)$$

In Eqs. (A·24)–(A·26), we have dropped the superscripts 'f' and 'h' in π^{ec} , π^{pc} , J^{ec} , J^{pc} , $\langle ft \rangle_{\text{eff}}^{\text{ec}}$, $\langle ft \rangle_{\text{eff}}^{\text{pc}}$, ζ^{ec} , and ζ^{pc} for simplicity.

The average energy of electron neutrinos produced by electron and positron captures is defined, in units of $m_e c^2$, as

$$\langle \epsilon_{\nu_e} \rangle^{\text{ec}} = \frac{J^{\text{ec}}}{I^{\text{ec}}}, \quad \langle \epsilon_{\bar{\nu}_e} \rangle^{\text{pc}} = \frac{J^{\text{pc}}}{I^{\text{pc}}}. \quad (\text{A}\cdot 27)$$

Then, the local neutrino energy emission rates by the electron and positron captures per unit volume is given by

$$Q_{\nu_e}^{\text{ec}} = \frac{\rho}{m_u} \left[X_p \langle \epsilon_{\nu_e} \rangle^{\text{ec},f} \lambda^{\text{ec},f} + \frac{X_A}{A} \langle \epsilon_{\nu_e} \rangle^{\text{ec},h} \lambda^{\text{ec},h} \right], \quad (\text{A}\cdot 28)$$

$$Q_{\bar{\nu}_e}^{\text{pc}} = \frac{\rho}{m_u} \left[X_n \langle \epsilon_{\bar{\nu}_e} \rangle^{\text{pc},f} \lambda^{\text{pc},f} + \frac{X_A}{A} \langle \epsilon_{\bar{\nu}_e} \rangle^{\text{pc},h} \lambda^{\text{pc},h} \right]. \quad (\text{A}\cdot 29)$$

Appendix B

— Neutrino pair processes —

In this section, we briefly summarize our treatment of pair processes of neutrino emission and give the explicit forms of $\gamma_{\nu_e \bar{\nu}_e}^{\text{pair}}$, $\gamma_{\nu_e \bar{\nu}_e}^{\text{plas}}$, $\gamma_{\nu_e \bar{\nu}_e}^{\text{Brems}}$, $\gamma_{\nu_x \bar{\nu}_x}^{\text{pair}}$, $\gamma_{\nu_x \bar{\nu}_x}^{\text{plas}}$, $\gamma_{\nu_x \bar{\nu}_x}^{\text{Brems}}$, $Q_{\nu_e \bar{\nu}_e}^{\text{pair}}$, $Q_{\nu_e \bar{\nu}_e}^{\text{plas}}$, $Q_{\nu_e \bar{\nu}_e}^{\text{Brems}}$, $Q_{\nu_x \bar{\nu}_x}^{\text{pair}}$, $Q_{\nu_x \bar{\nu}_x}^{\text{plas}}$, and $Q_{\nu_x \bar{\nu}_x}^{\text{Brems}}$ appeared in Eqs. (3·27), (3·28), (3·29) and (3·30), for the purpose of convenience.

B.1. Electron-positron pair annihilation

We follow Cooperstein et al.⁷⁸⁾ for the rate of pair creation of neutrinos by the electron-positron pair annihilation. The number emission rate of ν_e or $\bar{\nu}_e$ by the electron-positron pair annihilation can be written as

$$\gamma_{\nu_e \bar{\nu}_e}^{\text{pair}} = \frac{m_u}{\rho} \frac{C_{\nu_e \bar{\nu}_e}^{\text{pair}}}{36\pi^4} \frac{\sigma_0 c}{m_e^2 c^4} \frac{(k_B T)^8}{(\hbar c)^6} F_3(\eta_e) F_3(-\eta_e) \langle \text{block} \rangle_{\nu_e \bar{\nu}_e}^{\text{pair}}, \quad (\text{B}\cdot 1)$$

where $\sigma_0 \approx 1.705 \times 10^{-44} \text{cm}^{-2}$ and $C_{\nu_e \bar{\nu}_e}^{\text{pair}} = (C_V - C_A)^2 + (C_V + C_A)^2$ with $C_V = \frac{1}{2} + 2 \sin^2 \theta_W$ and $C_A = \frac{1}{2}$. The Weinberg angle is given by $\sin^2 \theta_W \approx 0.23$. Using the average energy of neutrinos produced by the pair annihilation,

$$\langle \epsilon_{\nu_e \bar{\nu}_e} \rangle^{\text{pair}} = \frac{k_B T}{2} \left(\frac{F_4(\eta_e)}{F_3(\eta_e)} + \frac{F_4(-\eta_e)}{F_3(-\eta_e)} \right), \quad (\text{B}\cdot 2)$$

the blocking factor $\langle \text{block} \rangle_{\nu_e \bar{\nu}_e}^{\text{pair}}$ is evaluated as

$$\langle \text{block} \rangle_{\nu_e \bar{\nu}_e}^{\text{pair}} \approx \left[1 + \exp \left(\eta_{\nu_e} - \frac{\langle \epsilon_{\nu_e \bar{\nu}_e} \rangle^{\text{pair}}}{k_B T} \right) \right]^{-1} \left[1 + \exp \left(\eta_{\bar{\nu}_e} - \frac{\langle \epsilon_{\nu_e \bar{\nu}_e} \rangle^{\text{pair}}}{k_B T} \right) \right]^{-1}. \quad (\text{B}\cdot 3)$$

The associated neutrino energy emission rate by the pair annihilation is given by

$$Q_{\nu_e \bar{\nu}_e}^{\text{pair}} = \frac{\rho}{m_u} \gamma_{\nu_e \bar{\nu}_e}^{\text{pair}} \langle \epsilon_{\nu_e \bar{\nu}_e} \rangle^{\text{pair}}. \quad (\text{B}\cdot 4)$$

Similarly, the number emission rate of ν_x or $\bar{\nu}_x$ by the electron-positron pair annihilation and the associated energy emission rate are given by

$$\gamma_{\nu_x \bar{\nu}_x}^{\text{pair}} = \frac{m_u}{\rho} \frac{C_{\nu_x \bar{\nu}_x}^{\text{pair}}}{36\pi^4} \frac{\sigma_0 c}{m_e^2 c^4} \frac{(k_B T)^8}{(\hbar c)^6} F_3(\eta_e) F_3(-\eta_e) \langle \text{block} \rangle_{\nu_x \bar{\nu}_x}^{\text{pair}}, \quad (\text{B}\cdot 5)$$

$$Q_{\nu_x \bar{\nu}_x}^{\text{pair}} = \frac{\rho}{m_u} \gamma_{\nu_x \bar{\nu}_x}^{\text{pair}} \langle \epsilon_{\nu_x \bar{\nu}_x} \rangle^{\text{pair}}, \quad (\text{B}\cdot 6)$$

where $C_{\nu_x \bar{\nu}_x} = (C_V - C_A)^2 + (C_V + C_A - 2)^2$. The average neutrino energy and the blocking factor are given by

$$\langle \epsilon_{\nu_x \bar{\nu}_x} \rangle^{\text{pair}} = \langle \epsilon_{\nu_e \bar{\nu}_e} \rangle^{\text{pair}} \quad (\text{B}\cdot 7)$$

and

$$\langle \text{block} \rangle_{\nu_e \bar{\nu}_e}^{\text{pair}} \approx \left[1 + \exp \left(\eta_{\nu_x} - \frac{\langle \epsilon_{\nu_x \bar{\nu}_x} \rangle^{\text{pair}}}{k_B T} \right) \right]^{-1} \left[1 + \exp \left(\eta_{\bar{\nu}_x} - \frac{\langle \epsilon_{\nu_x \bar{\nu}_x} \rangle^{\text{pair}}}{k_B T} \right) \right]^{-1}, \quad (\text{B}\cdot 8)$$

where note that $\eta_{\bar{\nu}_x} = \eta_{\nu_x}$.

B.2. Plasmon decay

We follow Ruffert et al.⁶³⁾ for the rate of pair creation of neutrinos by the decay of transversal plasmons. The number emission rate of ν_e or $\bar{\nu}_e$ can be written as

$$\gamma_{\nu_e \bar{\nu}_e}^{\text{plas}} = \frac{m_u}{\rho} \frac{C_V^2}{192\pi^3 \alpha_{\text{fine}}} \frac{\sigma_0 c}{m_e^2 c^4} \frac{(k_B T)^8}{(\hbar c)^6} \gamma_p^6 e^{-\gamma_p} (1 + \gamma_p) \langle \text{block} \rangle_{\nu_e \bar{\nu}_e}^{\text{plas}}, \quad (\text{B}\cdot 9)$$

where $\alpha_{\text{fine}} \approx 1/137$ is the fine-structure constant and $\gamma_p \approx 2\sqrt{(\alpha_{\text{fine}}/9\pi)(\pi^2 + 3\eta_e)}$. The blocking factor is approximately given by

$$\langle \text{block} \rangle_{\nu_e \bar{\nu}_e}^{\text{plas}} \approx \left[1 + \exp \left(\eta_{\nu_e} - \frac{\langle \epsilon_{\nu_e \bar{\nu}_e} \rangle^{\text{plas}}}{k_B T} \right) \right]^{-1} \left[1 + \exp \left(\eta_{\bar{\nu}_e} - \frac{\langle \epsilon_{\nu_e \bar{\nu}_e} \rangle^{\text{plas}}}{k_B T} \right) \right]^{-1}, \quad (\text{B}\cdot 10)$$

where

$$\langle \epsilon_{\nu_e \bar{\nu}_e} \rangle^{\text{plas}} = \frac{k_B T}{2} \left(2 + \frac{\gamma_p^2}{1 + 1\gamma_p} \right) \quad (\text{B}\cdot 11)$$

is the average energy of neutrinos produced by the plasmon decay. The associated neutrino energy emission rate is given by

$$Q_{\nu_e \bar{\nu}_e}^{\text{plas}} = \frac{\rho}{m_u} \gamma_{\nu_e \bar{\nu}_e}^{\text{plas}} \langle \epsilon_{\nu_e \bar{\nu}_e} \rangle^{\text{plas}}. \quad (\text{B}\cdot 12)$$

Similarly, the number emission rate of ν_x or $\bar{\nu}_x$ by the plasmon decay and the associated energy emission rate are given by

$$\gamma_{\nu_x \bar{\nu}_x}^{\text{plas}} = \frac{m_u}{\rho} \frac{(C_V - 1)^2}{192\pi^3 \alpha_{\text{fine}}} \frac{\sigma_0 c}{m_e^2 c^4} \frac{(k_B T)^8}{(\hbar c)^6} \gamma_p^6 e^{-\gamma_p} (1 + \gamma_p) \langle \text{block} \rangle_{\nu_x \bar{\nu}_x}^{\text{plas}}, \quad (\text{B}\cdot 13)$$

$$Q_{\nu_x \bar{\nu}_x}^{\text{plas}} = \frac{\rho}{m_u} \gamma_{\nu_x \bar{\nu}_x}^{\text{plas}} \langle \epsilon_{\nu_x \bar{\nu}_x} \rangle^{\text{plas}}, \quad (\text{B}\cdot 14)$$

where the average neutrino energy is $\langle \epsilon_{\nu_x \bar{\nu}_x} \rangle^{\text{plas}} = \langle \epsilon_{\nu_e \bar{\nu}_e} \rangle^{\text{plas}}$ and the blocking factor is given by

$$\langle \text{block} \rangle_{\nu_e}^{\text{pair}} \approx \left[1 + \exp \left(\eta_{\nu_x} - \frac{\langle \epsilon_{\nu_x \bar{\nu}_x} \rangle^{\text{pair}}}{k_B T} \right) \right]^{-1} \left[1 + \exp \left(\eta_{\bar{\nu}_x} - \frac{\langle \epsilon_{\nu_x \bar{\nu}_x} \rangle^{\text{pair}}}{k_B T} \right) \right]^{-1}. \quad (\text{B}\cdot 15)$$

B.3. Nucleon-nucleon bremsstrahlung

We follow Burrows et al.⁷⁹⁾ for the rate of pair creation of neutrinos by the nucleon-nucleon bremsstrahlung radiation. They derived the neutrino energy emission rate associated with the pair creation of ν_x or $\bar{\nu}_x$ by the nucleon-nucleon bremsstrahlung radiation without the blocking factor:

$$Q_{\nu_x \bar{\nu}_x}^{\text{Brems},0} = 3.62 \times 10^5 \zeta^{\text{Brems}} \left(X_n^2 + X_p^2 + \frac{28}{3} X_n X_p \right) \rho^2 \left(\frac{k_B T}{m_e c^2} \right)^{4.5} \langle \epsilon_{\nu_x \bar{\nu}_x} \rangle^{\text{Brems}}, \quad (\text{B}\cdot 16)$$

where $\zeta^{\text{Brems}} \sim 0.5$ is a correction factor and the average energy is

$$\langle \epsilon_{\nu_x \bar{\nu}_x} \rangle^{\text{Brems}} \approx 4.36 k_B T. \quad (\text{B}\cdot 17)$$

We multiply $Q_{\nu_x \bar{\nu}_x}^{\text{Brems},0}$ by the blocking factor,

$$\langle \text{block} \rangle_{\nu_x \bar{\nu}_x}^{\text{Brems}} \approx \left[1 + \exp \left(\eta_{\nu_x} - \frac{\langle \epsilon_{\nu_x \bar{\nu}_x} \rangle^{\text{Brems}}}{k_B T} \right) \right]^{-1} \left[1 + \exp \left(\eta_{\bar{\nu}_x} - \frac{\langle \epsilon_{\nu_x \bar{\nu}_x} \rangle^{\text{Brems}}}{k_B T} \right) \right]^{-1}, \quad (\text{B}\cdot 18)$$

to obtain the 'blocked' neutrino energy emission rate

$$Q_{\nu_x \bar{\nu}_x}^{\text{Brems}} = Q_{\nu_x \bar{\nu}_x}^{\text{Brems},0} \langle \text{block} \rangle_{\nu_x \bar{\nu}_x}^{\text{Brems}}. \quad (\text{B}\cdot 19)$$

The number emission rate of ν_x or $\bar{\nu}_x$ is readily given by

$$\gamma_{\nu_x \bar{\nu}_x}^{\text{Brems}} = 3.62 \times 10^5 \zeta^{\text{Brems}} \left(X_n^2 + X_p^2 + \frac{28}{3} X_n X_p \right) m_u \rho \left(\frac{k_B T}{m_e c^2} \right)^{4.5} \langle \text{block} \rangle_{\nu_x \bar{\nu}_x}^{\text{Brems}}. \quad (\text{B}\cdot 20)$$

Noting that the weak interaction coefficients of the bremsstrahlung radiation are¹¹¹⁾ $(1 - C_V)^2 + (1 - C_A)^2$ for the pair creation of $\nu_x \bar{\nu}_x$ and $C_V^2 + C_A^2$ for the pair creation of $\nu_e \bar{\nu}_e$, the number emission rate and the associated energy emission rate for ν_e or $\bar{\nu}_e$ may be written as

$$\gamma_{\nu_e \bar{\nu}_e}^{\text{Brems}} = \frac{C_V^2 + C_A^2}{(1 - C_V)^2 + (1 - C_A)^2} \gamma_{\nu_x \bar{\nu}_x}^{\text{Brems}}, \quad (\text{B}\cdot 21)$$

$$Q_{\nu_e \bar{\nu}_e}^{\text{Brems}} = \frac{C_V^2 + C_A^2}{(1 - C_V)^2 + (1 - C_A)^2} Q_{\nu_x \bar{\nu}_x}^{\text{Brems}}. \quad (\text{B}\cdot 22)$$

Appendix C

— Neutrino diffusion rates —

We follow Ref. 62) for the diffusive neutrino-number emission rate γ_ν^{diff} and the associated energy emission rate Q_ν^{diff} appeared in Eqs. (3·25) and (3·26). and present the explicit forms of them in the following for convenience. An alternative definition of the diffusion rates are found in Ref. 63).

C.1. Neutrino diffusion rates

To calculate the neutrino diffusion rates γ_ν^{diff} and Q_ν^{diff} , we first define neutrino diffusion time. In this paper, we consider cross sections for scattering on nuclei ($\sigma_{\nu A}^{\text{sc}}$), on free protons ($\sigma_{\nu p}^{\text{sc}}$), and on free neutrons ($\sigma_{\nu n}^{\text{sc}}$), and for absorption on free nucleons $\sigma_{\nu n}^{\text{ab}}$ for electron neutrinos and $\sigma_{\nu p}^{\text{ab}}$ for electron anti-neutrinos.

Ignoring the higher order correction terms in neutrino energy E_ν , these neutrino cross sections can be written in general as

$$\sigma(E_\nu) = E_\nu^2 \tilde{\sigma}, \quad (\text{C}\cdot 1)$$

where $\tilde{\sigma}$ is a 'cross section' in which E_ν^2 dependence is factored out. In practice, the cross sections contain the correction terms which cannot be expressed in the form of Eq. (C·1). We take account of these correction terms, approximating neutrino-energy dependence by temperature dependence according to

$$E_\nu \approx k_B T \frac{F_3(\eta_\nu)}{F_2(\eta_\nu)}. \quad (\text{C}\cdot 2)$$

The opacity is written as

$$\kappa(E_\nu) = \sum \kappa_i(E_\nu) = E_\nu^2 \sum \tilde{\kappa}_i = E_\nu^2 \tilde{\kappa}, \quad (\text{C}\cdot 3)$$

and optical depth is calculated by

$$\tau(E_\nu) = \int \kappa(E_\nu) ds = E_\nu^2 \int \tilde{\kappa} ds = E_\nu^2 \tilde{\tau}. \quad (\text{C}\cdot 4)$$

Then, we define neutrino diffusion time by

$$T_\nu^{\text{diff}}(E_\nu) \equiv a^{\text{diff}} \frac{\Delta x(E_\nu)}{c} \tau(E_\nu) = E_\nu^2 a^{\text{diff}} \frac{\tilde{\tau}^2}{c \tilde{\kappa}} = E_\nu^2 \tilde{T}_\nu^{\text{diff}}, \quad (\text{C}\cdot 5)$$

where the distance parameter $\Delta x(E_\nu)$ is given by

$$\Delta x(E_\nu) = \frac{\tau(E_\nu)}{\kappa(E_\nu)}. \quad (\text{C}\cdot 6)$$

Note that $\tilde{T}_\nu^{\text{diff}}$ can be calculated only using matter quantities. a^{diff} is a parameter which controls how much neutrinos diffuse outward and we chose it to be 3 following Ref. 63). For a larger value of a^{diff} , corresponding neutrino emission rate due to diffusion becomes smaller.

Finally, we define the neutrino diffusion rates by

$$\gamma_\nu^{\text{diff}} \equiv \frac{m_u}{\rho} \int \frac{n_\nu(E_\nu)}{T_\nu^{\text{diff}}(E_\nu)} dE_\nu = \frac{1}{a^{\text{diff}}} \frac{m_u}{\rho} \frac{4\pi c g_\nu}{(hc)^3} \frac{\tilde{\kappa}}{\tilde{\tau}^2} T F_0(\eta_\nu), \quad (\text{C}\cdot 7)$$

$$Q_\nu^{\text{diff}} \equiv \int \frac{E_\nu n_\nu(E_\nu)}{T_\nu^{\text{diff}}(E_\nu)} dE_\nu = \frac{1}{a^{\text{diff}}} \frac{4\pi c g_\nu}{(hc)^3} \frac{\tilde{\kappa}}{\tilde{\tau}^2} T^2 F_1(\eta_\nu). \quad (\text{C}\cdot 8)$$

C.2. Summary of cross sections

In this subsection, we briefly summarize the cross sections adopted in the present neutrino leakage scheme.

C.2.1. Neutrino nucleon scattering

The total ν - p scattering cross section σ_p for all neutrino species is given by

$$\sigma_{\nu p}^{\text{sc}} = \frac{\sigma_0}{4} \left(\frac{E_\nu}{m_e c^2} \right)^2 [(C_V - 1)^2 + 3g_A^2 (C_A - 1)^2], \quad (\text{C}\cdot 9)$$

where g_A is the axial-vector coupling constant $g_A \approx -1.26$. On the other hand, the total ν - n scattering cross section σ_n is

$$\sigma_{\nu n}^{\text{sc}} = \frac{\sigma_0}{16} \left(\frac{E_\nu}{m_e c^2} \right)^2 [1 + 3g_A^2]. \quad (\text{C}\cdot 10)$$

C.2.2. Coherent scattering of neutrinos on nuclei

The differential cross section for the ν - A neutral current scattering is written as¹¹⁸⁾

$$\frac{d\sigma_A^{\text{sc}}}{d\Omega} = \frac{\sigma_0}{64\pi} \left(\frac{E_\nu}{m_e c^2} \right)^2 A^2 [\mathcal{W}\mathcal{C}_{\text{FF}} + \mathcal{C}_{\text{LOS}}]^2 \langle \mathcal{S}_{\text{ion}} \rangle (1 + \cos \theta), \quad (\text{C}\cdot 11)$$

where θ is the azimuthal angle of the scattering and

$$\mathcal{W} = 1 - \frac{2Z}{A} (1 - 2\sin^2 \theta_W). \quad (\text{C}\cdot 12)$$

$\langle \mathcal{S}_{\text{ion}} \rangle$, \mathcal{C}_{LOS} , and \mathcal{C}_{FF} are correction factors due to the Coulomb interaction between the nuclei,¹¹²⁾ due to the electron polarization,¹¹³⁾ and due to the finite size of heavy nuclei.¹¹⁴⁾ Because it is known that the correction factor \mathcal{C}_{LOS} is important only for low neutrino energies,⁷⁹⁾ we consider only $\langle \mathcal{S}_{\text{ion}} \rangle$ and \mathcal{C}_{FF} .

The correction factor due to the Coulomb interaction between the nuclei is given by

$$\langle \mathcal{S}_{\text{ion}} \rangle = \frac{3}{4} \int_{-1}^1 d\cos \theta (1 + \cos \theta)(1 - \cos \theta) \mathcal{S}_{\text{ion}}. \quad (\text{C}\cdot 13)$$

Itoh et al.¹¹⁶⁾ presented a detailed fitting formula for the correction factor. However, the fitting formula is very complicated, we use a simple approximation based on Ref. 117).

\mathcal{S}_{ion} can be written approximately as¹¹⁷⁾

$$\mathcal{S}_{\text{ion}} \approx \frac{(qa_I)^2}{3\Gamma + f(\Gamma)(qa_I)^2} \quad (\text{C}\cdot 14)$$

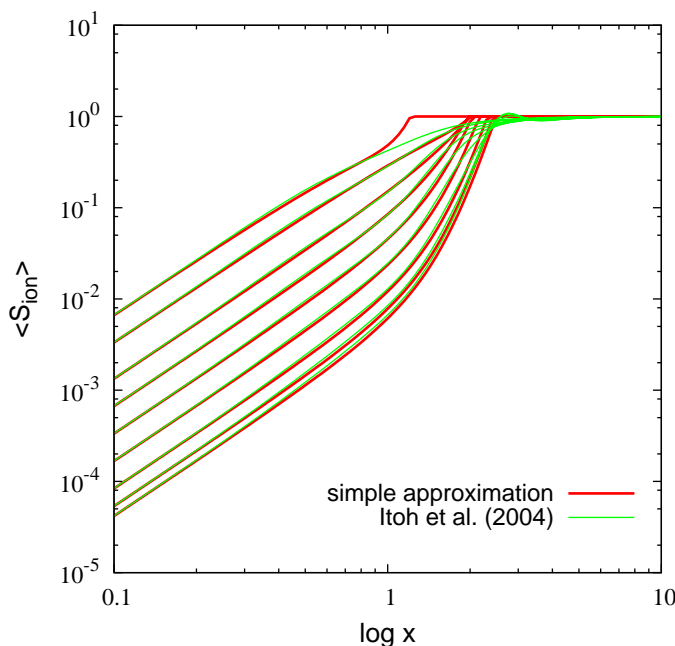


Fig. 11. Comparison of the ion-ion correction term, as a function of $x \equiv E_\nu a_I / (\hbar c)$, between our simplified estimation and a detailed fitting formula by Itoh et al. From the top to the bottom, the curves are for $\Gamma = 1, 2, 5, 10, 20, 40, 80, 125, 160$.

for ($qa_I \ll 1$), where $q = (2E_\nu / \hbar c) \sin(\theta/2)$, $a_I = (4\pi n_A / 3)^{-1/3}$ is the ion-sphere radius, n_A is the number density of a nucleus, and $\Gamma = (Ze)^2 / (a_I k_B T)$ is the conventional parameter that characterizes the strongness of the Coulomb interaction. $f(\Gamma)$ is given by¹¹⁶⁾

$$f(\Gamma) \approx 0.73317 - 0.39890\Gamma + 0.34141\Gamma^{1/4} + 0.05484\Gamma^{-1/4}. \quad (\text{C}\cdot 15)$$

The integration approximately gives for $x \equiv E_\nu a_I / (\hbar c) < 1$

$$\langle \mathcal{S}_{\text{ion}} \rangle \approx \frac{1}{6} \frac{1}{\Gamma} x^2 - \frac{1}{30} \frac{f(\Gamma)}{\Gamma^2} x^4 + \frac{1}{135} \frac{(f(\Gamma))^2}{\Gamma^3} x^6 - \frac{1}{567} \frac{(f(\Gamma))^3}{\Gamma^4} x^8 + \frac{1}{2268} \frac{(f(\Gamma))^4}{\Gamma^5} x^{10}. \quad (\text{C}\cdot 16)$$

To use this expression for the case of $x \geq 1$, we set the maximum value as $\langle \mathcal{S}_{\text{ion}} \rangle = \max(1, \langle \mathcal{S}_{\text{ion}} \rangle)$ where $\langle \mathcal{S}_{\text{ion}} \rangle = 1$ corresponds to the case without the correction. Note that x can be larger than unity^{*)}. In this case, the simple approximation on average underestimates the effect of the Coulomb interaction between the nuclei (see Fig. 11).

Figure 11 compares the correction term as a function of the parameter x calculated by our simple approximation and by a detailed fitting formula by Itoh et al.¹¹⁶⁾ For smaller values of Γ , the disagreements become prominent. Note that the typical value of Γ inside the collapsing core with $T \sim 1$ MeV, $\rho \sim 10^{12}$ g/cm³, $A = 56$ and $Z = 26$ (⁵⁶Fe) is $\Gamma \sim 47$.

^{*)} $x \sim (E_\nu / 27 \text{ MeV}) (\rho_{12} / A)^{-1/3}$ where ρ_{12} is the rest-mass density in units of 10^{12} g/cm³

C.2.3. Absorption on free neutrons

The total cross section of the absorption of electron neutrinos on free neutrons is given by¹¹⁸⁾

$$\sigma_n^{\text{ab}} = \sigma_0 \left(\frac{1 + 3g_A^2}{4} \right) \left(\frac{E_\nu + \Delta_{\text{np}}}{m_e c^2} \right)^2 \left[1 - \left(\frac{m_e c^2}{E_\nu + \Delta_{\text{np}}} \right) \right] W_M, \quad (\text{C}\cdot 17)$$

where $\Delta_{\text{np}} = m_n c^2 - m_p c^2$, and W_M is the correction for weak magnetism and recoil which is approximately given by

$$W_M \approx 1 + 1.1 \frac{E_\nu}{m_n c^2}. \quad (\text{C}\cdot 18)$$

Similarly, the total cross section of the absorption of electron anti-neutrinos on free protons is given by¹¹⁸⁾

$$\sigma_p^{\text{ab}} = \sigma_0 \left(\frac{1 + 3g_A^2}{4} \right) \left(\frac{E_{\bar{\nu}} - \Delta_{\text{np}}}{m_e c^2} \right)^2 \left[1 - \left(\frac{m_e c^2}{E_{\bar{\nu}} - \Delta_{\text{np}}} \right) \right] W_{\bar{M}}, \quad (\text{C}\cdot 19)$$

where $W_{\bar{M}}$ is approximately given by

$$W_{\bar{M}} \approx 1 - 7.1 \frac{E_{\bar{\nu}}}{m_p c^2}. \quad (\text{C}\cdot 20)$$

References

- 1) K. Hirata, et al., Phys. Rev. Lett. **58** (1987), 1490.
- 2) R. M. Bionta et al., Phys. Rev. Lett. **58** (1987), 1494.
- 3) W. D. Arnett, J. N. Bahcall, R. P. Kirshner, and S. E. Woosley, Ann. Rev. Astron. Astrophys. **27** (1989), 629.
- 4) A. Abramovici, et al., Science **256** (1992), 325.
- 5) F. Acernese, et al., Class. Quantum Grav. **21** (2004), S385.
- 6) B. Willke, et al., Class. Quantum Grav. **19** (2002), 1377.
- 7) M. Ando and the TAMA Collaboration, Class. Quantum Grav. **19** (2002), 1409.
- 8) K. Kotake, K. Sato, and K. Takahashi, Rep. Prog. Phys. **69** (2006), 971.
- 9) H.-Th. Janka, K. Langanke, A. Marek, G. Martínez-Pinedo, and B. Müller, Phys. Rep. **442** (2007), 38.
- 10) H. A. Bethe, Rev. Mod. Phys. **62** (1990), 801.
- 11) M. Rampp and H.-Th. Janka, Astrrophys. J. **539** (2000), L33.
- 12) A. Mezzacappa, M. Liebendörfer, O. E. B. Messer, W. R. Hix, F.-K. Thielemann, and S. W. Bruenn, Phys. Rev. Lett. **86** (2001), 1935.
- 13) T. A. Thompson, A. Burrows, and P. A. Pinto, Astrophys. J. **592** (2003), 434.
- 14) M. Rampp and H.-Th. Janka, Astron. Astrophys. **396** (2002), 361.
- 15) M. Liebendörfer, A. Mezzacappa, F.-K. Thielemann, O. E. B. Messer, W. R. Hix, and S. W. Bruenn, Phys. Rev. D **63** (2001), 103004.
- 16) K. Sumiyoshi, S. Yamada, H. Suzuki, H. Shen, S. Chiba, and H. Toki, Astrophys. J. **629** (2005), 922.
- 17) F. S. Kitaura, H.-Th. Janka, and W. Hillebrandt, Astron. Astrophys. **450** (2006), 345.
- 18) A. Marek and T. Th. Janka, Astrophys. J. **694** (2009), 664.
- 19) A. Burrows, E. Livne, L. Dessart, C. D. Ott, and J. Murphy, Astrophys. J. **640** (2006), 878.
- 20) H. Dimmelmeier, J. A. Font, and E. Müller, Astron. Astrophys. **388** (2002), 917; Astron. Astrophys. **393** (2002), 523.

- 21) R. Mönchmeyer, G. Schäfer, E. Müller, and R. E. Kates, *Astron. Astrophys.* **264** (1991), 417.
- 22) A. Burrows and J. Hayes, *Phys. Rev. Lett.* **76** (1996), 352.
- 23) E. Müller and H.-Th. Janka, *Astron. Astrophys.* **317** (1997), 140.
- 24) T. Zwerger and E. Müller, *Astron. Astrophys.* **320** (1997), 209.
- 25) K. Kotake, S. Yamada, and K. Sato, *Phys. Rev. D* **68** (2003), 044023; K. Kotake, S. Yamada, K. Sato, K. Sumiyoshi, H. Ono, and H. Suzuki, *Phys. Rev. D* **69** (2004), 124004.
- 26) C. D. Ott, A. Burrows, E. Livne, and R. Walder, *Astrophys. J.* **600** (2004), 834.
- 27) E. Müller, M. Rampp, R. Buras, H.-Th. Janka, and D. H. Shoemaker, *Astrophys. J.* **603** (2004), 221.
- 28) C. L. Fryer, D. E. Holz, and S. A. Hughes, *Astrophys. J.* **609** (2004), 288.
- 29) M. Shibata and Y. Sekiguchi, *Phys. Rev. D* **69** (2004), 084024; *Phys. Rev. D* **71** (2005), 024014.
- 30) Y. Sekiguchi and M. Shibata, *Phys. Rev. D* **71** (2005), 084013.
- 31) P. Cerdá-Durán, G. Faye, H. Dimmelmeier, J. A. Font, J. M^a. Ibáñez, E. Müller, and G. Schäfer, *Astron. Astrophys.* **439** (2005), 1033.
- 32) M. Shibata, Y. T. Liu, S. L. Shapiro, B. C. Stephens, *Phys. Rev. D* **74** (2006), 104026.
- 33) C. D. Ott, H. Dimmelmeier, A. Marek, H.-T. Janka, I. Hawke, B. Zink, and E. Schnetter, *Phys. Rev. Lett.* **98** (2007), 261101.
- 34) H. Dimmelmeier, C. D. Ott, H.-Th. Janka, A. Marek, and E. Müller, *Phys. Rev. Lett.* **98** (2007), 251101.
- 35) H. Shen, H. Toki, K. Oyamatsu, and K. Sumiyoshi, *Nucl. Phys. A* **637** (1998), 435; *Prog. Theor. Phys.* **100** (1998), 1013.
- 36) M. Liebendörfer, *Astrophys. J.* **633** (2005), 1042.
- 37) M. J. Rees, in *The future of theoretical physics and cosmology: celebrating Stephen Hawking's 60th birthday*, edited by G. W. Gibbons et al. (Cambridge University Press, Cambridge, 2003), p.217, (astro-ph/0401365).
- 38) J. E. McClintock and R. A. Remillard, in *Compact Stellar X-ray Sources*, edited by W. H. G. Lewin and van der Klis (Cambridge University Press, Cambridge, 2006), (astro-ph/0306213).
- 39) K. Sumiyoshi, S. Yamada, H. Suzuki, and S. Chiba, *Phys. Rev. Lett.* **97** (2006), 091101; K. Sumiyoshi, S. Yamada, and H. Suzuki *Astrophys. J.* **667** (2007), 382.
- 40) K. Nakazato, K. Sumiyoshi, and S. Yamada, *Astrophys. J.* **666** (2007), 1140.
- 41) Y. Sekiguchi and M. Shibata, *Prog. Theor. Phys.* **117** (2007), 1029.
- 42) Y. T. Liu, S. L. Shapiro, and B. C. Stephens, *Phys. Rev. D* **76** (2007), 084017.
- 43) S. R. Kulkarni et al., *Nature* **395** (1998), 663; T. J. Galama et al, *Nature* **395** (1998), 670.
- 44) J. Hjorth et al., *Nature* **423** (2003), 847; K. Z. Stanek et al., *Astrophys. J.* **591** (2003), L17; K. S. Kawabata et al., *Astrophys. J.* **593** (2003), L19.
- 45) M. Modjaz et al, *Astrophys. J.* **645** (2006), L21; J. Sollerman et al, *Astron. Astrophys.* **454** (2006), 503.
- 46) S. E. Woosley, *Astrophys. J.* **405** (1993), 273; B. Paczyński, *Astrophys. J.* **494** (1998), L45; A. MacFadyen and S. E. Woosley, *Astrophys. J.* **524** (1999), 262.
- 47) M. Shibata and S. L. Shapiro, *Astrophys. J.* **572** (2002), L39.
- 48) Y. Sekiguchi and M. Shibata, *Phys. Rev. D* **70** (2004), 084005.
- 49) S. Yamada, H. Th. Janka, and H. Suzuki, *Astron. Astrophys.* **344** (1999), 533.
- 50) M. Liebendörfer et al., *Astrophys. J. Suppl.* **150** (2004), 263.
- 51) R. I. Epstein and C. J. Pethick, *Astrophys. J.* **243** (1981), 1003.
- 52) K. A. van Riper and J. M. Lattimer, *Astrophys. J.* **249** (1981), 270.
- 53) K. A. van Riper, *Astrophys. J.* **257** (1982), 793.
- 54) S. A. Bludman, I. Lichtenstadt, and G. Hayden, *Astrophys. J.* **261** (1982), 661.
- 55) A. Ray, S. M. Chitre, and K. Kar, *Astrophys. J.* **285** (1984), 766.
- 56) E. A. Baron, J. Cooperstein, and S. Kahana, *Nucl. Phys. A* **440** (1985), 744.
- 57) J. Cooperstein, *Phys. Rep.* **163** (1988), 95.
- 58) K. Kotake, S. Yamada, and K. Sato, *Astrophys. J.* **595** (2003), 304.
- 59) C. D. Ott et al., *Astrophys. J.* **685** (2008), 1069.
- 60) H. A. Bethe, *Rev. Mod. Phys.* **62** (1990), 801.
- 61) Y. Sekiguchi 2007 *PhD thesis* (University of Tokyo).
- 62) S. Rosswog and M. Liebendörfer, *Mon. Not. R. Astron. Soc.* **342** (2003), 673.

- 63) M. Ruffert, H.-Th. Janka, and G. Schäfer, *Astron. Astrophys.* **311** (1996), 532.
- 64) H. A. Bethe and J. R. Wilson, *Astrophys. J.* **295** (1985), 14.
- 65) S. W. Bruenn, *Astrophys. J. Suppl.* **58** (1985), 771.
- 66) G. M. Fuller, W. A. Fowler, and M. J. Newman, *Astrophys. J.* **293** (1985), 1.
- 67) J. Cooperstein and J. Wambach, *Nucl. Phys. A* **420** (1984), 591.
- 68) Bowers R L and Wilson J R 1982 *Astrophys. J. Suppl.* **50** 115
- 69) E. Myra et al., *Astrophys. J.* **318** (1987), 744.
- 70) A. Mezzacappa and S. W. Bruenn, *Astrophys. J.* **405** (1993), 405.
- 71) E. Livne et al., *Astrophys. J.* **609** (2004), 277.
- 72) R. Buras et al., *Astron. Astrophys.* **447** (2006), 1049.
- 73) A. Burrows et al., *Astrophys. J.* **655** (2007), 416.
- 74) A. Mezzacappa and E. B. Messer, *J. Comp. Appl. Math.* **109** (1999), 281.
- 75) C. W. Misner and D. H. Sharp, *Phys. Rev.* **136** (1964), B571.
- 76) M. Liebendörfer, S. C. Whitehouse and T. Fischer, *Astrophys. J.* **698** (2009), 1174.
- 77) M. Shibata, Y. Sekiguchi, and R. Takahashi *Prog. Theor. Phys.* **118** (2007), 257.
- 78) J. Cooperstein et al., *Astrophys. J.* **309** (1986), 653.
- 79) A. Burrows et al., *Nucl. Phys. A* **777** (2006), 356.
- 80) Y. Sugahara and H. Toki, *Nucl. Phys. A* **579** (1994), 557.
- 81) e.g., R. Brockmann and R. Machliedt, *Phys. Rev. C* **42** (1990), 1965.
- 82) J. M. Lattimer and F. D. Swesty, *Nucl. Phys. A* **535** (1991), 331.
- 83) C. Ishizuka, A. Ohnishi, K. Tsunakihara, K. Sumiyoshi, and S. Yamada, *J. Phys. G* **35** (2008), 085201.
- 84) J. P. Cox and R. T. Giuli, *Principles of Stellar Structure volume 2.*, (Gordon & Breach, New York, 1968).
- 85) J. W. York, Kinematics and Dynamics of General Relativity, in *Sources of gravitational radiation*, edited by Smarr, L., (Cambridge University Press, Cambridge, 1979).
- 86) M. Shibata and T. Nakamura, *Phys. Rev. D* **52** (1995), 5428.
- 87) T. W. Baumgarte and S. L. Shapiro, *Phys. Rev. D* **59** (1999), 024007.
- 88) M. Alcubierre et al, *Int. J. Mod. Phys. D* **10** (2001), 273.
- 89) M. Shibata, *Phys. Rev. D* **67** (2003), 024033.
- 90) K. Kiuchi et al., *Phys. Rev. D* **80** (2009), 064037.
- 91) M. Alcubierre and B. Brügmann, *Phys. Rev. D* **63** (2001), 104006.
- 92) M. Shibata, *Astrophys. J.* **595** (2003), 992.
- 93) A. Kurganov and E. Tadmor, *J. Comp. Phys.* **160** (2000), 214.
- 94) S. E. Woosley, A. Heger, and T. A. Weaver, *Rev. Mod. Phys.* **74** (2002), 1015.
- 95) S. L. Shapiro and S. A. Teukolsky, *Black Holes, White Dwarfs, and Neutron Stars* (Wiley Interscience, New York, 1983).
- 96) M. Liebendörfer et al., *Astrophys. J.* **620** (2005), 840.
- 97) J. M. Lattimer and T. J. Mazurek, *Astrophys. J.* **246** (1981), 955.
- 98) A. Burrows and B. A. Fryxell, *Astrophys. J.* **418** (1993), L33.
- 99) M. Herant et al., *Astrophys. J.* **435** (1994), 339.
- 100) A. Burrows, J. Hayes, and B. A. Fryxell, *Astrophys. J.* **450** (1995), 830.
- 101) W. Keil, H.-Th. Janka, and E. Müller, *Astrophys. J.* **473** (1996), 111.
- 102) A. Mezzacappa et al., *Astrophys. J.* **493** (1998), 848.
- 103) L. Dessart et al., *Astrophys. J.* **645** (2006), 534.
- 104) M. Shibata and Y. Sekiguchi, *Phys. Rev. D* **68** (2003), 104020.
- 105) E. E. Flanagan and S. A. Hughes, *Phys. Rev. D* **57** (1998), 4535.
- 106) W. Hillebrandt, in *High Energy Phenomena around Collapsed Stars*, ed. F. Pacini, (Reidel, Dordrecht, 1987), p.73.
- 107) M. B. Aufderheide et al., *Astrophys. J.* **91** (1994), 389.
- 108) C. J. Horowitz, *Phys. Rev. D* **65** (2002), 043001.
- 109) J. L. Anderson and E. A. Spiegel, *Astrophys. J.* **171** (1972), 127.
- 110) K. S. Thorne, *Mon. Not. R. Astron. Soc.* **194** (1981), 439.
- 111) N. Itoh et al. *Astrophys. J. Suppl.* **102** (1996), 411.
- 112) C. J. Horowitz, *Phys. Rev. D* **55** (1997), 4577.
- 113) L. B. Leinson, V. N. Oraevsky, and V. B. Semikoz, *Phys. Lett. B* **209** (1988), 80.
- 114) D. L. Tubbs and D. N. Schramm, *Astrophys. J.* **201** (1975), 467; A. Burrows, T. J. Mazurek, and J. M. Lattimer, *Astrophys. J.* **251** (1981), 325

- 115) S. W. Bruenn and A. Mezzacappa, *Phys. Rev. D* **56** (1997), 7529.
- 116) N. Itoh et al. *Astrophys. J.* **611** (2004), 1041.
- 117) N. Itoh, *Prog. Theor. Phys.* **54** (1975), 1580.
- 118) A. Burrows and T. A. Thompson, in *Stellar Collapse*, ed. C. L. Fryer, (Kluwer Academic, Dordrecht, 2004); A. Burrows, S. Reddy, and T. A. Thompson, *Nucl. Phys. A* **777** (2006), 356.